Investigation of 3D Primary Human Airway Cell Culture as a Viable and Successful Model for Study of Respiratory Syncytial Virus Infection and Antiviral Drug Treatment.

Citation

McAllister, Nicole. 2020. Investigation of 3D Primary Human Airway Cell Culture as a Viable and Successful Model for Study of Respiratory Syncytial Virus Infection and Antiviral Drug Treatment.. Master's thesis, Harvard Extension School.

Permanent link

https://nrs.harvard.edu/URN-3:HUL.INSTREPOS:37364896

Terms of Use

Share Your Story

The Harvard community has made this article openly available.
Please share how this access benefits you. Submit a story .

Accessibility

Investigation of 3D Primary Human Airway Cell Culture as a Viable and Successful Model for

Study of Respiratory Syncytial Virus Infection and Antiviral Drug Treatment.

Nicole Victoria McAllister

A Thesis in the Field of Biology

for the Degree of Master of Liberal Arts in Extension Studies

Harvard University

March 2020

Abstract

Respiratory Syncytial Virus is almost universally experienced by the human population, infecting the airway and posing a significant risk to the very young and elderly populations in addition to immunocompromised individuals. Resulting in a Th2 immune response, RSV is most commonly associated with upper and lower respiratory tract infection and bronchiolitis in addition to coinfections such as influenza or pneumonia. EpiAirway, a 3D cell culture model of primary human tracheal and bronchial epithelial cells from MatTek, was used to test 5 laboratory and clinical strains of RSV. Four antiviral compounds with different mechanisms of action were tested in this model; PC786, GS-5806, RSV-604, and ALS-8112, with treatment given at the time of infection or delayed by 6 or 72 hours. qRT-PCR readout of viral load was the endpoint for all experiments, and cytokine concentration was measured using multiplex assays, both measured 5 days after addition of drug. Infection treated with RSV-604 or PC786 had a greater viral load reduction than treatment with GS-5806 or ALS-8112 across all viral strains tested. Delaying drug treatment appeared to decrease this reduction, and a similar trend was seen in tissue from asthmatic donors compared to normal tissue. These results were compared to similar viral testing run in 2D cell culture using a HEp-2 cell line, wherein comparable compound efficacy trends were seen when treatment was applied at the time of infection. After infection in EpiAirway tissue, IL-6, IP-10, and RANTES concentration levels increased in both normal and asthmatic samples. All cytokines tested with the exception of TSLP and RANTES were higher in asthma tissue than normal

tissue. Overall the EpiAirway system presents a useful and applicable 3D cell culture model to study RSV and offers numerous paths for future study to understand both the infection process and the efficacy of antiviral compounds.

Acknowledgments

My work on this project would not have been possible without the help and support of my thesis directors, Dr. Michael Rhodin and Dr. Carla Kim. Your advice, guidance, and time enabled me to complete my master's degree with confidence and allowed me to learn and achieve more than I thought possible. A special thank you as well to my thesis advisor Dr. James Morris, who has been helpful throughout the thesis process from the very beginning. MatTek Corporation and Meso Scale Diagnostics not only provided high-quality materials for this project but incredible customer service and troubleshooting throughout the process. I'd like to give thanks in particular to Brooke Knapp, Viktor Karetsky, Dr. Virginie Esain, and Sarah Rivest for their advice and assistance.

I am incredibly grateful to my employer Enanta Pharmaceuticals for allowing me to utilize their laboratory space and for providing funding for this project. Thank you to Dr. Yat Sun Or, Dr. Bryan Goodwin, Dr. Kai Lin, and Nathaniel Gardiner, J.D. for your support and interest in my work.

Table of Contents

List of Tables

List of Figures

Chapter I.

Introduction and Project Goals

Respiratory Syncytial Virus

Respiratory Syncytial Virus (RSV) is an enveloped, negative-sense, single-stranded ribonucleic acid (RNA) virus of the Mononegavirales order. First isolated from chimpanzees in 1995, this virus has annual seasonal outbreaks typically between the months of October and May, raising concerns for the particularly susceptible populations of young children, the immunocompromised, and the elderly (Blount, Morris, & Savage, 1956) (Rose, Wheatley, Langley, Gerber, & Haynes, 2018). Almost every individual has experienced an RSV infection by the age of 2, which can result in upper and/or lower respiratory tract infection, potentially leading to bronchiolitis or pneumonia (Centers for Disease Control and Prevention, 2018a). While RSV generally does not pose significant risk to the average healthy adult, a 2015 global survey of RSV-related lower respiratory infections estimated that there were 1.4 million hospital admissions, 27,300 deaths in hospital, and an overall mortality of 118,200 for infants under 6 months of age alone (Shi et al., 2017).

Three-Dimensional Cell Culture

The dynamic reciprocity model has been used to describe the crucial structural role of the extracellular matrix (ECM) in its interactions with surrounding cells, and how this relationship promotes tissue function (Bissell, Hall, & Parry, 1982). The ECM

describes the network of macromolecules that contributes to structural and biochemical

support of the surrounding cells, creating an environment which influences gene

expression, signaling pathways, and cell differentiation. Cells growing without the

presence of an ECM, such as *in vitro* two-dimensional (2D) cell culture, are far removed

from this natural structure and therefore not representative of a true tissue environment.

Factors such as surface stiffness, forced polarity from cell-to-cell contact only on a

singular plane, and uncontrolled cell spreading contribute to the 2D model having low

predictive power. In contrast, the presence of an ECM in three-dimensional (3D) culture

provides cell attachment along the entire surface of the cell, resulting in more realistic

shape and morphology.

      3D cell culture models, with their increased complexity, provide a more relevant

and representative environment for cell growth. There are 3 common systems for 3D

culture, where cells are grown on a matrix, in a matrix, or in suspension (Figure 1)

(Edmondson, Broglie, Adcock, & Yang, 2014). Often these systems utilize spheroids,

which are 3D spherical cellular aggregates that mimic natural cell responses and

interactions.
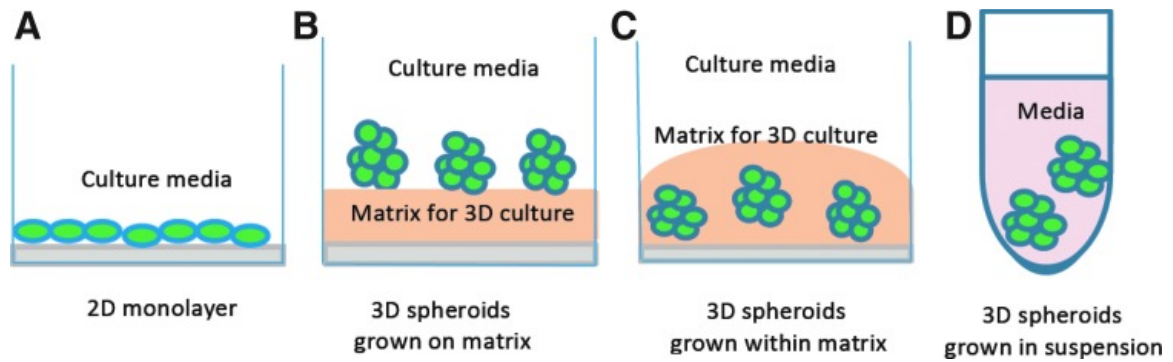
Figure 1. Cell Culture Models

"Schematic diagrams of the traditional 2D monolayer cell culture (A) and three typical 3D cell culture systems: cell spheroids/aggregates grown on matrix (B), cells embedded within matrix (C), or scaffold-free cell spheroids in suspension (D)" Adapted from *(Edmondson, Broglie, Adcock, & Yang, 2014).*

3D models allow researchers to experiment with factors such as interaction of different cell types, inclusion of immune cells, and cell self-organization into correct structures and morphology. The similarity of 3D culture to human patients is seen in both primary and immortalized cell lines (Sanyal, 2010). More complex 3D models such as organoids and organs-on-a-chip are considered to be the future of research in fields such as lung cancer, respiratory illness, and even air pollution. An organoid is a miniature, simplified 3D version of an organ produced *in vitro* with realistic anatomy. These models are designed to mimic the biological reality of gas exchange and absorption, interaction of multiple organ systems, inflammation, and therapeutic responses (Huh et al., 2010) (Coppeta et al., 2016).

RSV and Cytokines

In RSV-positive patients, disease progression results in an immune bias towards T helper type 2 (Th2)-like cytokines such as Interleukin (IL) 33, IL-8, thymic stromal lymphopoietin (TSLP), IL-6, periostin, and interferon alpha (IFN-α) (Vazquez et al., 2019). In many studies, these cytokines are associated with an increased risk of complications or more severe RSV symptoms, including IL-8, IFN-α, IL-3, and IL-33. In one study, young children with more serious RSV hospitalizations were seen to have increased levels of IL-6 and IL-8 along with decreased chemokine ligand 5 (CCL5 /RANTES) levels in plasma compared to less critical patients; 3.6 times more, 2.7 times more, and 3 times less respectively (Brand et al., 2013). In a study with 851 RSV patients under 5 years old, more critical illness was associated with 2.2 times higher IL-6 levels and 1.4 times higher INF-α levels in patient nasal washes compared to control patients (Tabarani et al., 2013). In one study, protein levels of IL-10 increased after RSV infection, with T helper cells (CD4$^+$ T cells) producing the majority in the lungs and peaking at 6 days post-infection (dpi) (Weiss, Christiaansen, Fulton, Meyerholz, & Varga, 2011). Conversely, a more recent study in RSV-infected children observed CD4$^+$ T cells producing lower levels of IL-2, IL-10, and IL-27 compared to healthy control children (Sananez et al., 2018).

Higher levels of TSLP, periostin, and IL-33 have been observed in infants with viral bronchiolitis compared to healthy infants, and detection of TSLP and IL-33 was more common in those with coinfections of RSV or Human Rhinovirus (HRV). Similar to IL-33 involvement in the initiation of the Th2 response, the matrix cellular protein periostin is included in many aspects of allergic inflammation and the Th2 phenotype

(Garcia-Garcia et al., 2017). In a study comparing air-liquid interface bronchial and nasal tissue cultures from asthmatic and healthy children, periostin expression was between 3.7 to 3.9-fold higher in cells from asthmatic patients measured by quantitative polymerase chain reaction (qPCR) (Lopez-Guisa et al., 2012). TSLP is a key factor in allergic airway responses and is linked to allergic asthma, with increased levels seen in asthmatic patient lung tissue (Garcia-Garcia et al., 2017). RSV-induced TSLP expression from epithelial cells has also been shown to have an important role in Th2 polarization, which causes enhanced immune response during reinfection with RSV (Han et al., 2012).

A study of infants less than 10 months old with acute RSV found highly elevated levels of interferon gamma-induced protein 10 (IP-10) in plasma compared to healthy infant controls, a phenomenon found in other conditions such as severe acute respiratory syndrome (SARS) and influenza (Roe, Bloxham, Cowburn, & O'Donnell, 2011). Experiments in mice have shown that expression of RANTES is correlated with RSV-related airway hyperreactivity. Levels were detectable at 1dpi, reducing by day 2, and increasing once again after day 6 before reaching peak levels by 10-12 dpi due to the inflammatory response (Kim K. Tekkanat, 2002). In a rat study, IL-33 was shown to reach elevated levels in neonate lung tissue after RSV infection, while no significant change was seen in adults. Expression of IL-33 was also found to be high in neonate airway epithelial cells (Saravia et al., 2015).

Cytokine studies have also been done from an *in vitro* perspective. A study from Bai et al. using a 3D human airway epithelial cell model with air-liquid interface harvested tissue and media for qPCR analysis, secreted chemokine and cytokine assessment, and gene expression. Gene expression analysis showed RANTES was

expressed differently in asthmatic versus non-asthmatic tissue before and after rhinovirus

infection (Bai et al., 2015). Chemokines RANTES and chemokine ligand 1 (CX3CL

1/Fractalkine) have been associated with asthma. Fractalkine is a chemokine involved in

both chemoattraction and adhesion which competes with the RSV G protein CX3C motif

for interaction and binding, and therefore can influence infection and immune response

(Harcourt et al., 2006). IP-10 was shown to significantly increase in asthmatic tissues

infected with rhinovirus. Overall, 32 analytes tested in the study from Bai et. al had

different expression before and after rhinovirus infection but showed no difference with

regards to asthmatic versus normal tissue. This list included IL-10, IFN-α, IL-7, IL-6, and

IL-8 with post-infection $\log_2$ fold increases of 4.9, 6.1, 2.1, 2.6, and 0.7 respectively (Bai

et al., 2015).

Background of the Problem

RSV is a common virus which targets the respiratory epithelium and causes

inflammation, often leading to upper and/or lower respiratory tract infection. In healthy

adults, it results in symptoms similar to the common cold before being cleared by the

immune system within 1-2 weeks. This leaves those with weakened or underdeveloped

immune systems particularly vulnerable to more severe effects from infection, even

leading to hospitalization and death. The virus has 2 subtypes which circulate every

season, RSV-A and RSV-B, with studies disagreeing over whether one is consistently

more transmissible or more inclined towards severe disease than the other. The subtypes

are differentiated by their G protein variability and neutralizing antibody specificity. A

2017 study of hospitalized RSV-positive children suggested for that season, RSV-only

bronchitis had a higher risk of requiring intensive care treatment for those with RSV-A

(Laham et al., 2017). Within the immunocompromised patient population, a 2019 risk assessment showed those with the highest risk of severe RSV infection were lung transplant recipients, heart/lung transplant recipients, allogeneic stem cell transplant recipients, and severe combined immunodeficiency (SCID) patients (Science, Akseer, Asner, & Allen, 2019).

While there is a very present need for RSV prevention and treatment, Palivizumab (Synagis) is the sole product approved in the United States as a prophylactic. However, treatment is limited to high-risk infants due to its significant cost. This monoclonal antibody for the RSV fusion protein was shown in the 1998 IMpact-RSV Study to have a 55% reduction in RSV-related hospitalizations, and in a 2017 Weighted Regression Analysis was shown to have an effectiveness of 58% (The IMpact-RSV Study Group, 1998) (Anderson, Carosone-Link, Yogev, Yi, & Simoes, 2017). While Ribavirin is an approved antiviral, there are safety concerns for both patient and medical personnel which dissuade it from being a common treatment for non-critically ill patients. Among these are reported bronchospasms, conjunctivitis, anemia, and teratogenic potential (Krilov, 2002). Remaining medical efforts are focused on supportive care to ease patient symptoms. Future vaccine and antiviral research efforts to create drugs with higher effectiveness against the virus are in development.

The virus gets its name from the formation of syncytial cells prior to cell lysis, though this phenomenon is considered unique to the *in vitro* infection. These multinucleated cells are formed from the fusion of cell membranes. Common cell types used for *in vitro* research and drug discovery related to RSV are immortalized human epithelial type 2 (HEp-2) and adenocarcinomic human alveolar basal epithelial (A549)

cells as well as primary human bronchial epithelial cells (HBECs). For *in vivo* study,

animal models are limited in their relevance and pathogenesis, and are often semi-

permissive to the virus in addition to having a significant cost. These include cotton rats,

mice, ferrets, guinea pigs, hamsters, chinchillas, neonatal lambs, and African Green

Monkeys as well as a calf model for bovine RSV (Taylor, 2017).

Prior Research

Lung and airway cell culture research has been explored in a 3D setting, with

emphasis on cell differentiation and replicating the body environment. Immortalized

A549 cells grown on a rat lung-derived matrix showed increased levels of matrix

degradation enzymes, cell proliferation, and apoptosis when compared to A549 2D

culture (Mishra et al., 2012). Primary human airway epithelial (HAE) cells from patients

displayed the biomarkers keratin 5 (CK5), tight junction protein 1 (ZO-1), and pan-

cytokeratin (PCK) as well as the development of cilia when grown in 3D culture -

features normal to this cell type that do not appear in 2D culture (Y. X. Chen et al.,

2018). Differentiation of HBECs into mucus-producing glandular acini, another aspect of

the human respiratory tract, was similarly observed when the cells were grown on a 3D

culture membrane matrix (Wu, Peters-Hall, Bose, Pena, & Rose, 2011).

A tissue-like assembly model for the human lung which utilized rotating wall

vessel bioreactors has been successfully infected with RSV, and budding virus was

visualized with scanning electron microscopy (Goodwin, McCarthy, Cohrs, & Kaufer,

2015). Another complex model generated lung bud organoids from pluripotent stem cells

which could be grown in Matrigel 3D culture, and infection with RSV demonstrated cell

injury similar to symptoms observed during *in vivo* lung infection (Y. W. Chen et al.,

2017). The generation and RSV infection of human airway organoids has also been described by Sachs et al., a process which requires access to patient lung tissue samples (Sachs et al., 2019).

A 2018 study by Mirabelli et al. investigated RSV-A Long infection and antiviral treatments in the Epithelix 3D cell culture model using fully differentiated HAE with an air-liquid interface. This model included both ciliated and mucus-producing cells, though lacking cells of the immune system. Fusion protein-inhibitor GS-5806 was given before or after infection to explore the effects of time of compound addition, with viral rebound being measured. Compounds with different mechanisms of action were tested therapeutically, with viral rebound once again being used as an indicator of compound potency and efficacy. Unlike 2D cell culture with HEp-2 cells, infection with RSV-A Long in this 3D model did not result in visible cytopathic effect (CPE). Therefore, ciliary beat frequency (CBF) and viral load as determined by quantitative reverse transcription polymerase chain reaction (qRT-PCR) were used as indicators to measure the degree of infection (Mirabelli et al., 2018).

A 2018 abstract reported that a fully differentiated small airway epithelium 3D model could be successfully infected with a clinical isolate of the RSV-B subtype; decreased mucin clearance was observed without damage to tissue integrity. Ribavirin treatment given either apically or basally was able to inhibit viral replication. In addition, the treatment prevented (to a degree) the decreased mucin clearance caused by viral infection (Huang et al., 2018).

The EpiAirway model utilized in this project has been used to examine functional, structural, and mechanistic properties that account for Human Parainfluenza Virus 3

(HPIV3) growth in an *in vivo*-like environment versus monolayer 2D tissue culture (Xu et al., 2013). The EpiAirway model was also used to show that clinical isolates of HPIV have different, more stable fusion protein machinery than viruses adapted to grow in traditional 2D cell culture (Palmer et al., 2014). Additionally, EpiAirway HAE cells used to passage HPIV3 clinical isolates were shown to result in genetic selection similar to that which occurs in a human host, and may avoid mutations that occur only in immortalized cell culture (Palermo et al., 2016). In a 2012 study, the EpiAirway model was used to demonstrate the ability of a dendrimer to reduce infectivity of RSV-A2 (Donalisio et al., 2012). In a 2016 study, RSV-A strains A2 VR-1302, A2 VR-1540, A Long, and clinical isolate A2001 3-12 along with RSV-B VR-1580 were tested in EpiAirway normal bronchial epithelial cells, and Ribavirin was found to reduce viral replication (Jung, Choi, Westover, Smee, & Day, 2016).

Research Question and Aims

The goal of 3D cell culture is to provide a more realistic *in vitro* model for biomedical research, particularly with regards to virology-related studies. This is an environment in which cell growth, differentiation, and infection of cells can occur with morphology, structure, and organization that more closely resembles a human host. Lung and airway epithelium are useful tissues to grow in a 3D model due to the multiple cell types, air interface, and presence of cilia and mucus which also occur *in vivo*.

There has been limited study of RSV in the 3D culture model, particularly in the realm of antiviral testing. 3D culture is a useful step in research, allowing for more extensive compound testing before the *in vivo* stage of development. This work hypothesizes that both laboratory and clinical RSV strains will propagate successfully in

the chosen 3D cell culture model and demonstrate CPE similar to symptoms seen in human hosts. Antiviral compound treatment is expected to have less efficacy in disease models when compared to normal tissue. This research will investigate the use of 3D cell culture for pre-clinical RSV antiviral testing using the EpiAirway model from MatTek Corporation, in which cell aggregates are grown on a matrix (mimicking the functions of the ECM) and exposed to an air-liquid interface. In previous reports it has been demonstrated that this model can be successfully infected with RSV and treated (Donalisio et al., 2012) (Jung, Choi, Westover, Smee, & Day, 2016).

This 3-aim study further explores the ability of RSV to infect cells in a 3D culture setting, including a range of viral subtypes such as RSV-B VR-995, RSV-A2, and RSV clinical isolates. In particular, the effectiveness of antiviral compounds in the 3D cell culture model will be tested to determine if this model is a legitimate and useful *in vitro* method to test compound efficacy. Multiple endpoints will be analyzed to determine which aspects of the model are best suited for measuring extent of viral infection and degree of viral inhibition/cell protection. The model will also be used to test for differences in viral replication and compound efficacy between normal and diseased tissue models.

Specific Aim 1

The goal of this aim is to demonstrate that the EpiAirway 3D cell culture model is viable and useful for infection and antiviral studies with both laboratory and clinical strains of RSV.

Summary. In this aim, laboratory and clinical RSV strains from both the A and B subtypes will be used for infection. Four compounds with different mechanisms of action

and established efficacy against RSV *in vitro* will be used to test antiviral effectiveness in the 3D model; PC786 (Pulmocide, a non-nucleoside L-protein inhibitor) (Coates et al., 2017), GS-5806 (Gilead Sciences, Inc., a fusion protein inhibitor) (Mackman et al., 2015), RSV-604 (Arrow Therapeutics, Novartis, presumed N-protein inhibitor) (Henderson et al., 2007), and ALS-8112 (Alios BioPharma, nucleoside L-protein inhibitor) (Deval et al., 2015). The effectiveness of these compounds will be compared to their performance in HEp-2 2D cell culture. In addition, compound efficacy against A versus B RSV subtypes will be compared within each culture type.

Rationale and Hypothesis. Based on both published and unpublished research performed at Enanta Pharmaceuticals, laboratory strains RSV-A Long and RSV-B VR-955 have been shown to successfully infect HBECs in a 2D cell culture setting (Rhodin et al., 2016) (Rhodin et al., 2018). However, there is limited data of RSV infection in a 3D cell culture model, particularly with RSV-B and clinical isolate strains. Due to the increased cell-to-cell contact and realistic organization, it is hypothesized that higher viral loads will be recovered from the 3D culture model. It has also been shown that certain antivirals such as RSV-604 perform better in primary HBECs than immortalized HEp-2 cells (Rhodin et al., 2016) (Rhodin et al., 2018). Despite this, it is predicted that due to improved viral replication, the antiviral compounds will have a half maximal effective concentration (EC_{50}) greater than or equal to that seen in a 2D cell culture model. In addition, it is hypothesized that compounds with a significantly higher efficacy in one subtype of RSV in 2D culture will show the same pattern in 3D culture.

Specific Aim 2

The goal of this aim is to determine if alternate treatment methods influence compound efficacy in a 3D cell culture environment.

Summary. In this aim, methods of compound treatment will be varied to determine if there is a significant impact on extent of infection and/or compound efficacy.

Rationale and Hypothesis. The conditions under which compounds are tested can dramatically affect their efficacy, and whether those conditions mimic the real body environment can affect the predictive power of *in vitro* results for later *in vivo* studies. Depending on the mechanism of action for certain drugs, the method of delivery influences the ability of the drug to have its maximum effect. The polarization of the airway epithelium *in vivo* allows for functional tight junctions and distribution of proteins and lipids. This structure is replicated in the 3D culture model, which allows study of compound delivery on a heterogenous cell population. This is especially relevant for RSV infection, since the ciliated apical surface of airway cells is exposed to airflow and mucus which interact with external pathogens.

If it is possible to alter compound delivery in the EpiAirway model, it is hypothesized that compounds intended for oral or intravenous delivery (GS-5806, RSV-604, and ALS-8112) will perform better when treated basally, and compounds intended for inhaled delivery (PC786) will perform better when tissue is treated apically – which is expected to be demonstrated by lower viral load.

Given the model's similarity to *in vivo* conditions, it is hypothesized that compound addition will impact efficacy depending on what point during infection the compound is delivered. For this version of experimentation, it is hypothesized that fusion

inhibitor GS-5086 will have the greatest loss of activity when added after infection while PC786, which acts post-viral entry, will have the smallest loss of activity.

Specific Aim 3

The goal of this aim is to identify differences in RSV infection and compound treatment effectiveness in 3D cell culture of diseased EpiAirway tissue.

Summary. In this aim, donor tissue from patients with asthma will be used in the 3D cell culture model. Progress of RSV infection will be observed to note if differences in CPE or viral load are present compared to infection of normal tissue. Antiviral treatment results will be compared to those in normal donor tissue to see if compound effectiveness is impaired in the disease model.

Rationale and Hypothesis. RSV is a very common infection, and the majority of severe disease, hospitalizations, and deaths occur in vulnerable populations. Having the ability to test both viral infection and antiviral efficacy in cells with a diseased phenotype is useful to understand how the virus and treatments interact in this environment. Asthma and chronic obstructive pulmonary disease (COPD) in particular are respiratory disease conditions that are associated with RSV infection or more severe symptoms (Centers for Disease Control and Prevention, 2018b). It is hypothesized that a greater viral load will be observed after infection of tissue from a diseased host when compared to normal tissue. In addition, it is theorized that all antiviral compounds will show decreased efficacy in the diseased model compared to normal tissue. RSV-promoted inflammation in the respiratory tract is thought to contribute to symptoms such as asthma and wheezing, therefore it is predicted that infection of diseased tissue will result in higher levels of proinflammatory cytokines than normal tissue (Bueno et al., 2011).

14

Significance of Research

3D culture is highly useful in research due to its correlation with cells'
environment, morphology, structure, differentiation, and interaction in the human body.
Different 3D models may be implemented across the stages of the drug discovery
process. This is especially useful with regards to the medical and pharmaceutical fields,
wherein body-chemical interactions are essential for the progress of successful disease
treatment. Experiments in more complex and realistic cell culture allow potential
products to be more thoroughly tested before expensive *in vivo* animal studies and human
clinical trials. This has far-reaching implications that could save laboratories time,
money, and other negative impacts of compounds failing further down the pipeline. This
study will explore if the EpiAirway 3D cell culture model can effectively be used to
study the course of RSV infection as well as test antiviral treatments in an environment
that more closely mimics infection in a human host than more traditional 2D culture
systems.

An ideal 3D cell culture model would be applicable to both normal and diseased
cell environments. Experimentation in primary cell disease models could be an indicator
of how antivirals may perform in future target populations whose RSV infection may be
more difficult to treat due to coinfection, chronic illness condition (such as asthma or
COPD), or immune system complications. Some studies have also indicated RSV
bronchiolitis as a high independent risk factor for individuals developing asthma or
sensitivity to inhaled allergens up to age seven (Sigurs, Bjarnason, Sigurbergsson, &
Kjellman, 2000). Having the ability to test RSV antivirals *in vitro* using diseased primary

cells could be a very useful indicator if a treatment will be efficacious in these

populations.

Definition of Terms

Table 1. Definition of Terms

2D (two-dimensional) cell culture	Cells adhere to and spread on a flat coated surface, often plastic
3D (three-dimensional) cell culture	Cells adhere to and grow in three dimensions, either with or without a scaffold
1/2/3/5/6/7/8/10/12 dpi	1/2/3/5/6/7/8/10/12 days post-infection
0/1/6/48 hpi	0/1/6/48 hours post-infection
A549 cells	An immortal cell line originating from cancerous human lung tissue
CO_2	Carbon dioxide
CCL5	Also known as RANTES, chemotactic protein which plays an active role in recruiting leukocytes
$CD4^+$ T cells	T helper cells
Cytotoxic concentration 10/50 (CC_{10}/CC_{50})	Cytotoxic concentration required for reduction of cell viability by 10%/50%
CI A	RSV clinical isolate of the A subtype
CI B	RSV clinical isolate of the B subtype
Ciliary beat frequency (CBF)	The measure of the rate at which the cilia of a tissue of interest beat or wave
CK5	Keratin 5; a marker for breast and lung cancer
COPD	Chronic obstructive pulmonary disease
CX3C	Chemokine family composed of CX3CL1
CX3CL1	Chemokine ligand 1, known as fractalkine
Cytopathic effect (CPE)	Structural change in host cell as a result of viral infection
Degrees Celsius (°C)	Unit of measuring temperature
DMEM	Dulbecco's Modified Eagle's Medium
DMEM F12	Dulbecco's Modified Eagle Medium: Nutrient Mixture F-12
DMSO	Dimethyl sulfoxide
Extracellular matrix (ECM)	3D network of extracellular macromolecules that provide structural and biochemical support
FBS	Fetal bovine serum
fg	Femtogram

Half maximal effective concentration/effective concentration 90 (EC_{50}/EC_{90})	Concentration of a drug which results in a response halfway between the baseline and maximum/90% of the maximum response
HEp-2 cells	Human Epithelial Type 2 cell: A cell line originally derived from a human laryngeal carcinoma, but later found to be indistinguishable from HeLa cells by PCR DNA analysis - immortalized cervical cancer cells
HPIV/HPIV3	Human Parainfluenza Virus/Human Parainfluenza Virus type 3
Human airway epithelium (HAE) cells	Primary cells from the human airway epithelium
Human bronchial epithelial cells (HBECs)	Primary cells from the human bronchial epithelium
HRV	Human rhinovirus
IL-2	Interleukin 2, regulates activity of white blood cells
IFN-$\alpha2\alpha$	Interferon alpha-2, involved in innate immunity
IL-3	Interleukin 3, produced by T cells and mast cells
IL-6	Interleukin 6, pro- and anti-inflammatory cytokine
IL-7	Interleukin 7, hematopoietic growth factor
IL-8	Interleukin 8, produced by macrophages and epithelial cells
IL-10	Interleukin 10, anti-inflammatory cytokine
IL-33	Interleukin 33, ligand for IL-1 family receptor
IL-27	Interleukin 27, expressed by antigen presenting cells
In vitro	Study/process performed outside the normal biological context
In vivo	Study/process performed in a living organism
IP-10	Also known as CXCL10, interferon gamma-induced protein 10
LDH	Lactate dehydrogenase, enzyme found in living cells
mL	Milliliter
mm	Millimeter
MSD	Meso Scale Diagnostics/Meso Scale Discovery. Acronym represents both the company and their ELISA-like method of using electrochemiluminescence for detection
Multiplicity of infection (MOI)	The ratio of infectious viral particles for each cell
nm	Nanometer
PBS	Phosphate-buffered saline
PCK	Pan-cytokeratin, marker for the differentiation of epithelial and mesothelial cells
PFU	Plaque forming units
pg	Picogram

(Quantitative) reverse transcription polymerase chain reaction/(q)RT-PCR	Process by which to detect, characterize and quantify RNA
Respiratory Syncytial Virus (RSV)	A virus that attacks the respiratory tract
RNA	Ribonucleic acid
RSV-A	A subtype of RSV
RSV-A2	A strain of the RSV-A subtype often used in research
RSV-B	A subtype of RSV
RSV-B VR-955	RSV-B Washington, a strain of the RSV-B subtype
RV-A16	Human rhinovirus, species A, type 16
Severe acute respiratory syndrome (SARS)	Respiratory illness caused by a coronavirus
Severe combined immunodeficiency (SCID)	Wherein the patient lacks both $CD4^+$ and $CD8^+$ cells
TEER	Transepithelial/transendothelial electrical resistance
Th2	T helper type 2
TSLP	Thymic stromal lymphopoietin, plays a role in maturing T cell populations
μL	Microliter
ZO-1	Tight junction protein-1

Chapter II.

Materials and Methods

Included in this chapter is an overview of the methods utilized for experiments throughout this project. Infection of all viral stocks was done based off a PFU (plaque forming units) per mL titer previously determined by plaque assay in house at Enanta Pharmaceuticals (data not shown). Clinical isolates were provided to Enanta Pharmaceuticals by Dr. Pedro Piedra, Baylor University.

2D Cell Culture Infection

HEp-2 cells were seeded into the inner 60 wells of a 96-well plate at 8,000 cells per well in a volume of 50 µL using growth medium (Dulbecco's Modified Eagle's Medium (DMEM) without phenol red, 1% L-Glutamine, 1% Penicillin-Streptomycin, 1% nonessential amino acids, 10% heat-inactivated FBS (fetal bovine serum)). The outer wells of the plate were filled with 120 µL of DMEM with 1% Penicillin-Streptomycin to act as a thermal and evaporative moat around the test wells. Twofold serial dilutions of the compounds were added to the wells in a total volume of 25 µL. Infection using a multiplicity of infection (MOI) of 0.1 in a volume of 25 µL occurred just after addition of compound, raising the total well volume to 100 µL. An equivalent percentage of sucrose was added to the uninfected control to account for sucrose used as the viral stabilizer. All wells had a dimethyl sulfoxide (DMSO) concentration of 0.5%. Plates were incubated at

37 degrees Celsius (°C) and 5% carbon dioxide (CO_2) for 5 days before being frozen at -80°C.

3D Cell Culture Model

The 3D cell culture model used in this study is the EpiAirway standard AIR-100 culture tissue by MatTek Corporation, which is composed of primary human tracheal and bronchial epithelial cells. MatTek is responsible for isolation of epithelial cells from lung tissue, cell expansion, and cryopreservation. Upon order, cells are seeded onto tissue culture inserts, and time is allowed for differentiation and stratification before shipment of the multilayer tissue to the customer. During all cell culture and experimentation for this project, the tissue had apical exposure to air and basolateral exposure to media and any compounds. The media used for culture is DMEM with epidermal growth factors and anti-fungal/bacterial agents, ordered from MatTek. This model is most similar to the schematic diagram B seen in Figure 1, though EpiAirway consists of aggregates grown on matrix rather than spheroids. The 3D structure of EpiAirway includes basal cells, mucus-producing goblet cells, tight junctions, and functioning cilia (Figure 2).

All tissue handling was done with autoclave-sterilized forceps, and all liquid added to tissue inserts was done by pipetting down the side of the insert. The samples used for all normal cell culture were from a 23-year-old Caucasian male donor, and the samples used for all asthmatic cell culture were from a 9-year-old black female donor.
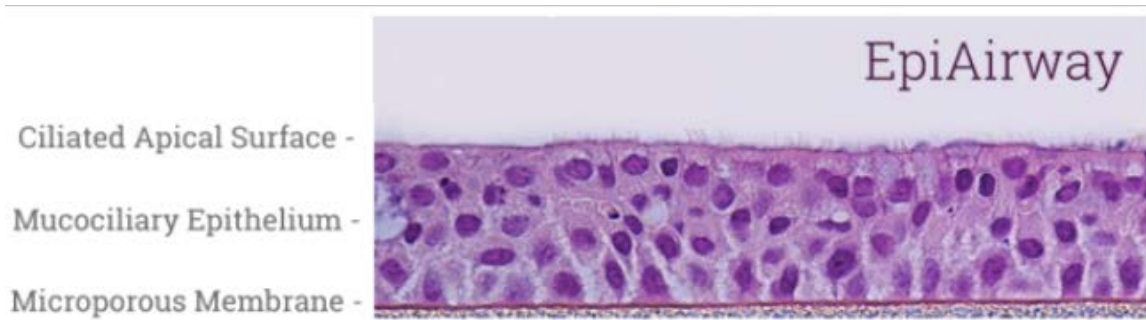
Figure 2. EpiAirway Tissue Structure

Histological diagram of the EpiAirway 3D cell culture model. Adapted from (MatTek Corporation, 2019b).

Culture and Infection

Upon day of receipt tissues were removed from agarose and placed into 6-well plates with 1 mL cold medium before incubating overnight at 37°C and 5% CO_2. The next day tissues were transferred to hanging top plates with wells containing 5 mL of pre-warmed medium (Figure 3). Every 2-3 days medium was replaced, and the apical tissue surface was washed every 7 days with 400 µL of transepithelial/transendothelial electrical resistance (TEER) buffer. Figures showing EpiAirway tissue during culture can be found in Appendix 2.

On the day of infection, the medium in each well was replaced. To wash the apical tissue surface, 400 µL of TEER buffer was added to each cell culture insert, and then aspirated without disturbing the tissue. Each insert was filled with 350 µL of media containing 3.11×10^4 PFU of virus based on viral titer. Control tissues received 350 µL of media; adding sucrose to account for the viral stock stabilizer was found to have no evident effect on viral load or cell health (data not shown). After a 1-hour incubation at

37°C and 5% CO_2, media was aspirated, and tissues were washed once with 400 μL

TEER buffer. Culture continued as described above until sample collection at 5dpi.
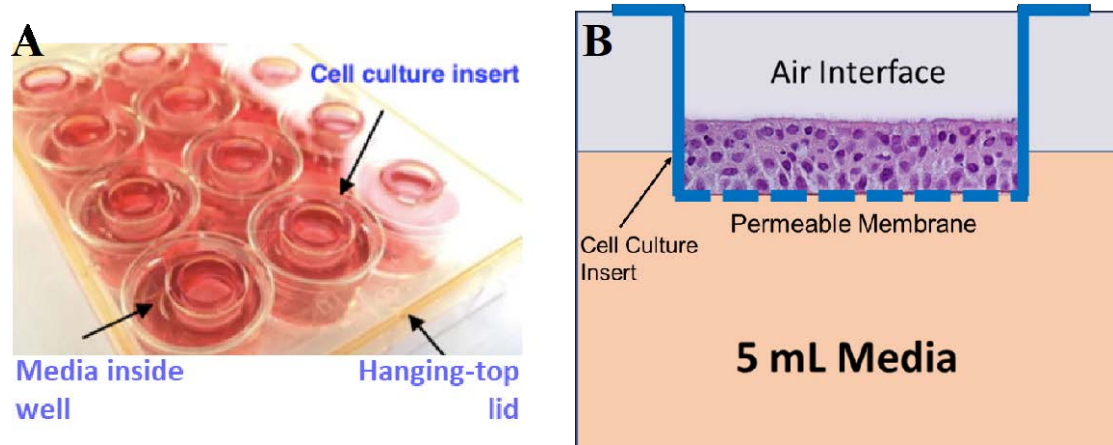
Figure 3. Hanging Top Plate Setup

Panel A. "The hanging-top lid on top of the bottom plate containing media" Adapted from (MatTek Corporation, 2019c). Panel B. Diagram of well in hanging-top plate, cross-section. Image of tissue structure adapted from (MatTek Corporation, 2019b).

Compound Treatment

Upon time of treatment, 5 mL of fresh medium containing compound was added to the wells of the hanging top plate. Medium had a concentration of 0.01% DMSO for PC786, GS-5806, and untreated controls or 0.1% DMSO for RSV-604 and ALS-8112. The differing concentration of DMSO was found to have no evident effect on viral load or cell health (data not shown). All medium changes contained fresh compound. Compound dilution curves consisted of 5 concentrations, serially diluted threefold. All samples were run in biological triplicate at minimum.

Time-of-Addition Assay

Infection and cell culture were run as described above. Fresh medium was added to wells at the time of infection, and fresh medium with compound was added either 6 hours or 3 days after infection. Samples were collected 5 days after the addition of compound. All samples were run in biological triplicate.

qRT-PCR Analysis

For 3D plates, the membrane was removed from the insert, taking care to include all visible residual tissue and mucus, and placed in a tube containing 400 µL of lysis buffer and 1.4 mm ceramic beads (Figure 4). Homogenization was done using the Bead Ruptor 24 from Omni International; tissues were processed for 30 seconds. RNA was extracted and isolated from the tissue using the RNAqueous Total RNA Isolation Kit and following the MatTek "Isolation of Total RNA from MatTek Tissue Models" protocol. For 2D plates, the Ambion RNAqueous-96 Automated Kit was used to extract RNA from the whole well, including supernatant. After extraction of all plates, qRT-PCR was run to determine viral load using the Applied Biosystems TaqMan RNA-to-CT 1-Step Kit and an assay standard with known concentrations. The primer/probes set for the N gene were as follows: (RSV-A: forward - CATCCAGCAAATACACCATCCA, reverse - TTCTGCACATCATAATTAGGAGTATCAA, probe - CGGAGCACAGGAGAT; and RSV-B: forward - CTGTCATCCAGCAAATACACTATTCA, reverse - GCACATCATAATTGGGAGTGTCA, probe - CGTAGTACAGGAGATAAT). Temperature conditions were 48ºC for 30 minutes, 95ºC for 10 minutes, and 40 cycles of 95ºC for 15 seconds and 50ºC for 1 minute.

Figure 4. Removal of EpiAirway Permeable Membrane

Depiction of the permeable membrane being removed from an EpiAirway cell culture insert for analysis. Adapted from (MatTek Corporation, 2014).

Cell Viability

Cell viability was measured using the lactate dehydrogenase (LDH) Cytotoxicity Detection kit from Takara Bio, which measures LDH released from cells upon damage to or rupture of the cell membrane. A positive control was made by adding 350 µL of a 0.5% Triton X-100 solution to a cell culture insert and incubating at 37°C and 5% CO_2 for at least 3 hours. This represented total cell death, while untreated tissue represented full cell health. Samples from the well media were used for this assay in biological triplicate at minimum, from infected, uninfected, treated, and untreated tissues. Absorbance was measured using a spectrometer at 492 nm with a reference wavelength of 650 nm. Percent cytotoxicity was calculated using the equation

$$\frac{\text{Sample signal} - \text{Untreated signal}}{\text{Cell death signal} - \text{Untreated signal}} \times 100.$$

Plaque Assay

EpiAirway tissue was infected using methods described above, and on days 1-10 post-infection the apical surface was washed with 500 µL of phosphate-buffered saline (PBS), which was frozen at -80°C. A 12-well culture plate was seeded with $0.55e^6$ HEp-2

cells per well in 1.5 mL of growth medium and incubated at 37°C and 5% CO_2 to settle overnight. The next day, growth medium was aspirated, and 500 µL of diluted apical wash sample was added. Each sample had a 1:2 dilution and three 1:10 serial dilutions added to the plate. Plates were incubated at 37°C and 5% CO_2 for at least 1 hour with occasional shaking. After infection period virus was aspirated and 1.5 mL of pre-warmed overlay (0.3% agarose in DMEM F12 medium) was added to each well. Plates were incubated at 37°C and 5% CO_2 for 8 days, when 1 mL of a 1% formaldehyde solution in PBS was added to each well and plates incubated at room temperature overnight. Once cells were fixed plates were flicked to remove agarose, washed gently with water, and 1.5 mL of a 1% neutral red solution in water was added to each well. Once sufficiently dyed, neutral red was removed, and plates gently washed with water. Plaques were counted using a dissection microscope and back-calculations were made to determine titer.

Cytokine Analysis

Medium from EpiAirway wells was collected at 5dpi and frozen at -80°C, with all samples run in biological triplicate at minimum. R-PLEX singleplex assays from Meso Scale Diagnostics (MSD) were used to measure the concentration of RANTES and Periostin. A 10-spot U-PLEX multiplex assay from MSD was used to measure the concentration of fractalkine, IFN-$\alpha2\alpha$, IL-2, IL-6, IL-7, IL-8, IL-10, IL-33, IP-10, and TSLP. To maximize coating, linker-coated antibody solution was left on plates overnight shaking at 4°C. Samples were measured neat for all analytes except for IL-8, where a 1:10 dilution was required. Both R-PLEX and U-PLEX assays came supplied with calibrator standards containing a pre-measured concentration of each analyte, and a

volume of standard was added to the cell media for use as a positive control. Untreated, uninfected cells were used as a reference. Cytokine concentrations were calculated using Discovery Workbench 4.0 software using the Meso Scale Discovery (MSD) instrument.

Statistical Analysis

Compound EC_{50} and effective concentration 90 (EC_{90}) were calculated based on percent viral inhibition using the XLFit 4-parameter logistic model 200 in Microsoft Excel. Infected untreated wells were used as a control. Maximum viral load reduction for each run was calculated by dividing the average untreated viral load of that run by the viral load at the highest level of inhibition for each compound. Log_{10} reduction was calculated by taking the log_{10} of this value. Fold shift of cytokine concentrations between conditions was calculated by dividing the concentration in infected cells by that in uninfected cells, or by dividing the concentration in asthmatic tissue by that in normal tissue. The log_2 fold shift was calculated by taking the log_2 of this value. Comparisons between relevant conditions were done using a 2-tailed T-test assuming unequal variance, using an alpha of 0.05. Outliers were determined as values falling above or below 1.5 times the interquartile range.

Chapter III.

Results

This chapter contains a summary of the results from all 3 aims of the project. For full data tables, see Appendix 1.

Specific Aim 1

The goal of this aim was to demonstrate infection and antiviral studies in the EpiAirway 3D model with laboratory and clinical strains of RSV, while comparing these results to similar studies conducted in 2D cell culture with a HEp-2 cell line.

2D Culture Compound Screen

The compounds of interest were successfully tested in HEp-2 2D culture. The overall trend for compound effectiveness across viruses was RSV-604 and PC786 having the greatest reduction in viral load at the point of maximum inhibition, while ALS-8112 and GS-5806 had the lowest reduction (Figure 5). For RSV-A, RSV-B VR-955, and RSV-A2 infection, PC786 ($p<0.01$) and RSV-604 ($p<0.01$, $p<0.05$, $p<0.01$ respectively) treatment had greater viral load reduction than ALS-8112-treated tissues. Against RSV-A2, PC786 and RSV-604 had greater reduction than GS-5806 ($p<0.05$). For RSV-A clinical isolate 121301343, PC786 and RSV-604 resulted in a greater reduction than ALS-8112 ($p<0.01$, $p<0.05$ respectively), while PC786 also had greater reduction than

GS-5806 (p<0.05). For RSV-B clinical isolate 65848 infection, RSV-604 had greater

viral load reduction than ALS-8112 treatment (p<0.05) (Figure 5).
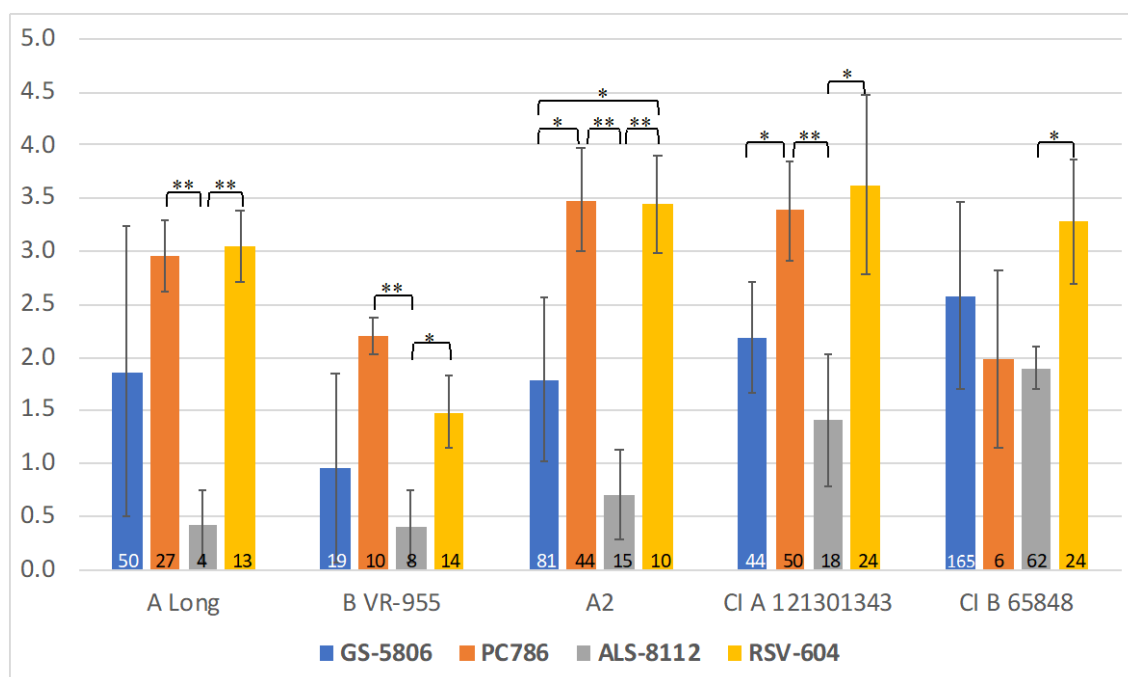
Figure 5. Average Log_{10} Viral Load Reduction in HEp-2 2D Culture

*Viral load log_{10} reduction at the point of maximum viral inhibition. Error bars represent standard deviation. Numbers on the bottom of each bar indicate maximum concentration the compound was tested up to, relative to fold-EC_{50} within each virus. * indicates significance p<0.05, ** indicates significance p<0.01.*

The trend in 2D culture EC_{50} was GS-5806 treatment resulting in the lowest value

across the viral strains tested, while ALS-8112 gave the highest EC_{50} (Table 2). PC786

demonstrated greater effectiveness against RSV-A strains than RSV-B. All compounds

except for ALS-8112 reached 100% viral inhibition against RSV-A Long, though this is

likely due to the fact that the compound was only tested up to 4 times EC_{50} (Figure 6).

Table 2. Compound Efficacy in HEp-2 2D Cell Culture

RSV Strain	GS-5806		PC786		ALS-8112		RSV-604	
	EC_{50} (nM)	Viral load Reduction	EC_{50} (nM)	Viral load Reduction	EC_{50} (nM)	Viral load Reduction	EC_{50} (nM)	Viral load Reduction
A Long	1.6 ± 0.9 (4)	1.9 ± 1.4	4.7 ± 2.7	3 ± 0.3	29,324 ± 18,719	0.4 ± 0.3	2,304 ± 856	3 ± 0.3
B VR-955	4.2 ± 1.1	0.9 ± 0.9	122 ± 26	2.2 ± 0.2	30,617 ± 25,619	0.4 ± 0.3	2,150 ± 311	1.5 ± 0.3
A2	1 ± 0.2	1.8 ± 0.8	2.9 ± 0.8	3.5 ± 0.5	7,952 ± 920	0.7 ± 0.4	2,882 ± 712	3.4 ± 0.5
CI A 121301343	1.8 ± 1	2.2 ± 0.5	2.6 ± 1	3.4 ± 0.5	6,608 ± 5,521 (4)	1.4 ± 0.6	1,276 ± 405	3.6 ± 0.8
CI B 65848	0.5 ± 0.3	2.6 ± 0.9	23 ± 4.4	2 ± 0.8	1,947 ± 832 (5)	1.9 ± 0.2	1,241 ± 328	3.3 ± 0.6

Table depicting efficacy of antiviral treatments across 5 laboratory and clinical strains of RSV with respect to EC_{50} and $\log_{10}$ viral load reduction at the point of maximum inhibition. All treatments were given at the time of infection. Values shown as average ± standard deviation. N=3 for all samples except when signified by number in parentheses. CI A and CI B stand for clinical isolate of the RSV-A subtype and clinical isolate of the -B subtype respectively.
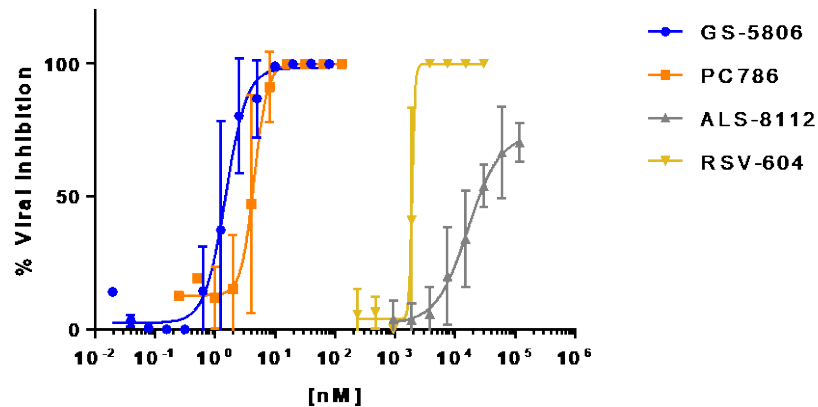
Figure 6. RSV-A Long Viral Inhibition Curves in HEp-2 2D Culture

Viral inhibition curves of compounds tested against RSV-A Long, drawn using [inhibitor] vs. response 4 parameter variable slope model in GraphPad Prism. Error bars represent standard deviation.

3D Culture Compound Screen

EpiAirway experiments without compound treatment demonstrated that this 3D model supports RSV infection across multiple strains. RSV-A Long viral load from tissue collection increased from the time of infection through 10dpi, indicating successful viral replication (Figure 7). Any potential viral load in the well media was negligible, with an estimated 1% of inoculum getting into well media likely via areas of membrane not covered by cells. This viral level was no longer detectable after the first medium replacement (data not shown). In addition, measuring viral load of the inoculum and tissue harvested after the 1-hour viral incubation demonstrated that the inoculum was successfully washed off the tissue (Figure 7). The 1-hour post-infection (hpi) viral load was also compared to those detected after experimentation. The $\log_{10}$ fold viral load increase for assays ending 5dpi and 8dpi over the 1hpi viral load was 2.4 and 3.3 respectively. Tissue harvested at 3dpi contained a lower viral load than those harvested at 5 or 8dpi ($p<0.01$, $p<0.05$ respectively). In addition, viral load at 5dpi was lower than the viral load at 8dpi ($p<0.05$) (Table 3). The detectable virus was shown to be infectious, as the PFU/mL in apical washes of the tissue increased over the course of infection from 1dpi through 10dpi (Figure 8).

Table 3. EpiAirway Tissue Viral Load Through 10dpi

Time Post-Infection	Average Viral Load	N
0 hours	$4.5e8 \pm 5.6e^7$	2
1 hour	$1.3e^5$	1
3 days	$7.2e^6 \pm 2.7e^6$	3
5 days	$3.0e^7 \pm 2.5e^7$	23
8 days	$2.7e^8 \pm 2.6e^8$	10
10 days	$3.5e^8 \pm 1.1e^8$	6

RSV-A Long viral load as measured by qRT-PCR through 10dpi. Each N represents 1 tissue except the 0hpi point, which is solely the viral inoculum with no tissue
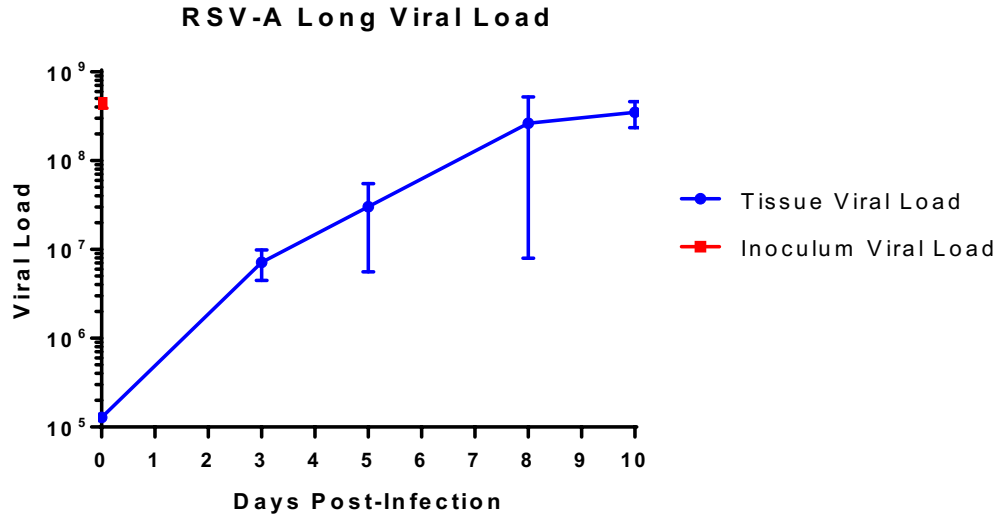
Figure 7. RSV-A Long Viral Load in EpiAirway Tissue

RSV-A Long viral load measured by qRT-PCR through 10dpi. Bars indicate standard deviation.
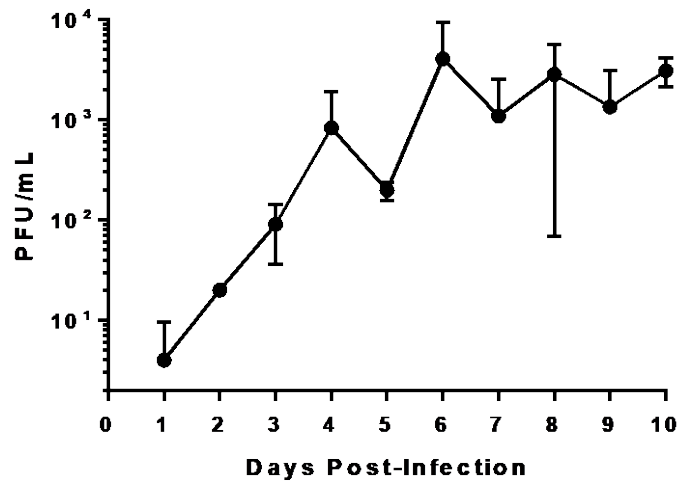
Figure 8. PFU per mL in Apical Washes of EpiAirway Tissue

PFUs in apical washes of EpiAirway tissue collected on days 1-10 post-RSV-A Long infection.

Further experiments confirmed the ability of the tested compounds to treat RSV in the EpiAirway 3D model. For all treatment groups across RSV-A Long, RSV-B VR-955, RSV-A2, clinical isolate RSV-A 121301343, and clinical isolate RSV-B 65848, there was a decrease in viral load at 5dpi compared to infected, untreated tissues ($p<0.01$, $p<0.05$, $p<0.05$, $p<0.05$, $p<0.01$ respectively). This was true when comparing viral load at maximum inhibition or the average viral load at points above 50% viral inhibition. The exception was GS-5806 treatment against clinical isolate A 121301343, which was only significant at the point of maximum viral inhibition.

The overall trend for compound effectiveness across viral strains was RSV-604 and PC786 having the greatest reduction in viral load, while ALS-8112 and GS-5806 had the smallest reduction (Table 4). This can be observed in the RSV-A Long inhibition curves, where RSV-604 and PC786 are the only compounds to plateau at 100% inhibition (Figure 9). For several conditions, the reduction of viral load at maximum inhibition differed when comparing compound treatments. Against RSV-A Long, PC786 treatment resulted in a greater reduction than ALS-8112 ($p<0.05$). With RSV-B VR-955 infection, RSV-604 treatment caused a greater reduction than GS-5806 ($p<0.05$). Against RSV-A2 infection, PC786 treatment resulted in a greater reduction than GS-5806 or ALS-8112 ($p<0.01$), and RSV-604 had a greater reduction than GS-5806 ($p<0.05$). For RSV clinical isolate B 65848, RSV-604 had a greater reduction than treatment with either GS-5806 or ALS-8112 ($p<0.05$) (Figure 10). There was no significant difference between compound treatments against RSV-A clinical isolate 121301343.

Table 4. Compound Efficacy in Normal EpiAirway Tissue

GS-5806

RSV Strain	EC_{50} (nM)	EC_{90} (nM)	Log_{10} Max Viral Reduction
A Long	2.5 ± 2.3	9.5 ± 9.3	1.3 ± 0.04
B VR-955	0.1 ± 0.1 (4)	1.9	1.1 ± 0.3
A2	0.2 ± 0.2 (4)	0.4 ± 0.3	1.3 ± 0.5
CI A 121301343	1.5 ± 1 (4)	3.1 ± 0.4	1.4 ± 0.8
CI B 65848	0.7 ± 0.5	1.6 ± 0.2	1.2 ± 0.4

PC786

EC_{50} (nM)	EC_{90} (nM)	Log_{10} Max Viral Reduction
1.5 ± 0.7	2.8 ± 1.6	2.2 ± 0.4
21 ± 1.3	31 ± 5.2	1.5 ± 0.6
0.5 ± 0.1	1.1 ± 0.2	3.3 ± 0.3
1.7	2.1 ± 0.4	2.4 ± 0.8
7 ± 5	26 ± 7.6	2.1 ± 0.5

ALS-8112

RSV Strain	EC_{50} (nM)	EC_{90} (nM)	Log_{10} Max Viral Reduction
A Long	2,492 ± 2,109	8,176 ± 7,161	1.2 ± 0.3
B VR-955	1,050 ± 1,086	6,499 ± 3,659	1.4 ± 0.4
A2	612 ± 296	4,658 ± 3,595	1.8 ± 0.3
CI A 121301343	1,707 ± 644	6,977 ± 7,084	1.6 ± 0.4
CI B 65848	831 ± 456	1,098	1.3 ± 0.5

RSV-604

EC_{50} (nM)	EC_{90} (nM)	Log_{10} Max Viral Reduction
402 ± 153	461 ± 155	2.4 ± 1.2
310 ± 140	484 ± 75	2.2 ± 0.4
210 ± 152	377 ± 218	3 ± 0.7
341 ± 134	653 ± 200	2.2 ± 0.7
513 ± 33	555 ± 28	3 ± 0.5

Table depicting compound efficacy of antiviral treatments across 5 laboratory and clinical strains of RSV with respect to EC_{50}, EC_{90}, and viral load log_{10} reduction, the latter using the point of maximum viral inhibition as reference. All treatments were given at the time of infection. Values shown as average ± standard deviation. If no standard deviation is given, viral inhibition curves did not allow for exact value determination for all replicates. N=3 for all samples except when signified by number in parentheses.
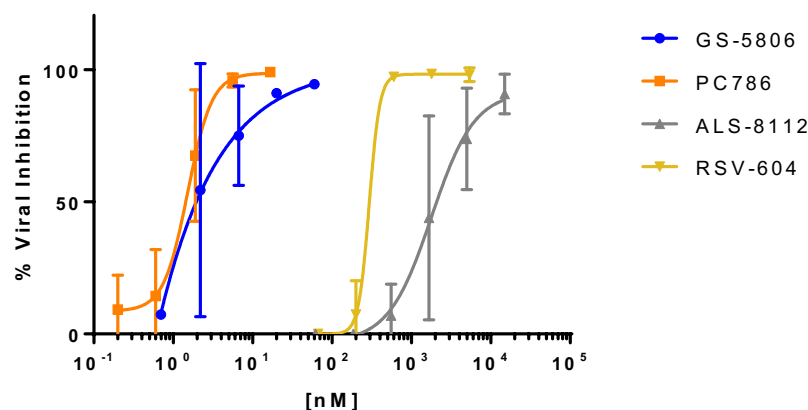
Figure 9. RSV-A Long Viral Inhibition Curves in EpiAirway Model

Viral inhibition curves of compounds tested against RSV-A Long in EpiAirway, drawn using [inhibitor] vs. response 4 parameter variable slope model in GraphPad Prism. Error bars represent standard deviation.
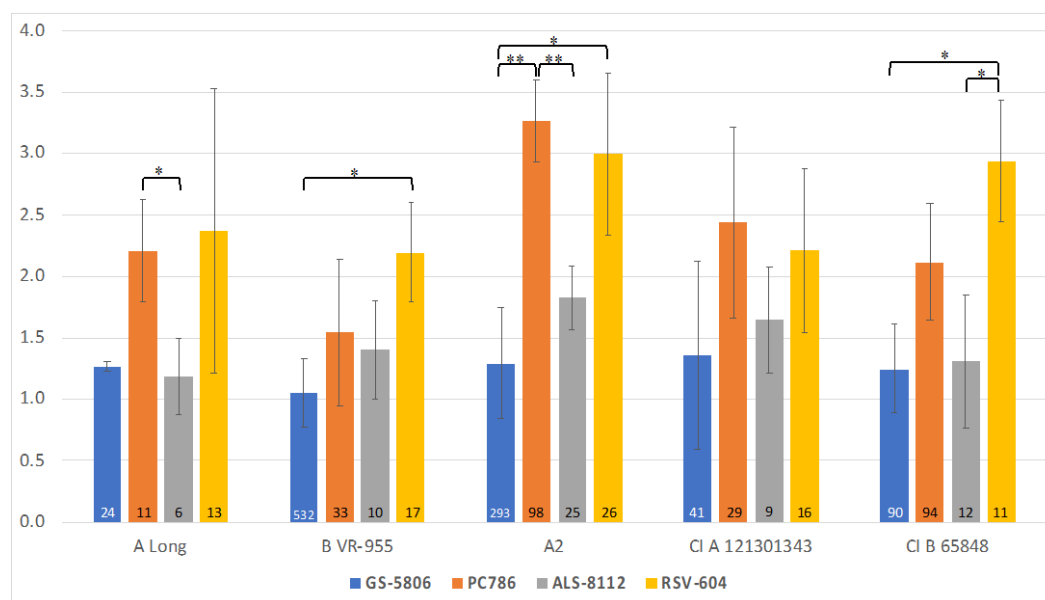
Figure 10. Average Log_{10} Viral Load Reduction in Normal EpiAirway Tissue

Viral load log_{10} reduction at the point of maximum viral inhibition. Numbers on the bottom of each bar indicate maximum concentration the compound was tested up to, relative to fold-EC_{50} within each virus. Error bars represent standard deviation.
* indicates significance p<0.05, ** indicates significance p<0.01.

As with 2D culture, GS-5806 treatment resulted in the lowest EC_{50} across the viruses tested, while ALS-8112 treatment resulted in the highest EC_{50}. PC786 also had greater efficacy against RSV-A strains than RSV-B strains. There were also some differences between 2D and 3D results, such as treatment with RSV-604 and ALS-8112 resulting in lower EC_{50}s in the 3D model than in HEp-2 2D culture (Table 5). Viral load reduction was often similar between 2D and 3D culture. Exceptions included viral load reduction of RSV-A clinical isolate 121301343, which was about 1-log_{10} lower in 3D culture compared to 2D culture with PC786 and RSV-604 treatment. Viral load reduction of RSV-B clinical isolate 65848 was also 1-log_{10} lower in 3D culture compared to 2D culture with GS-5806 treatment (Table 6). No statistical analysis was used to directly compare 2D and 3D results due to the differences between the models.

Table 5. Compound EC_{50} in HEp-2 2D vs. EpiAirway 3D Cell Culture

RSV Strain	EC_{50} (nM)							
	GS-5806		PC786		ALS-8112		RSV-604	
	2D	3D	2D	3D	2D	3D	2D	3D
A Long	1.6 ± 0.9	2.5 ± 2.3	4.7 ± 2.7 (4)	1.5 ± 0.7	29,324 ± 18,719	2,492 ± 2,109	2,304 ± 856	402 ± 153
B VR-955	4.2 ± 1.1	0.1 ± 0.1 (4)	122 ± 26	21 ± 1.3	30,617 ± 25,619	1,050 ± 1,086	2,150 ± 311	310 ± 140
A2	1 ± 0.2	0.2 ± 0.2 (4)	2.9 ± 0.8	0.5 ± 0.1	7,952 ± 920	612 ± 296	2,882 ± 712	210 ± 152
CI A 121301343	1.8 ± 1	1.5 ± 1 (4)	2.6 ± 1	1.7	6,608 ± 5,521 (4)	1,707 ± 644	1,276 ± 405	341 ± 134
CI B 65848	0.5 ± 0.3	0.7 ± 0.5	23 ± 4	7 ± 5	1,947 ± 832 (5)	831 ± 456	1,241 ± 328	513 ± 33

Table comparing EC_{50} of compounds across 5 laboratory and clinical strains of RSV in HEp-2 2D cell culture and EpiAirway 3D cell culture. All treatments were given at the time of infection. N=3 for all samples except where specified by number in parentheses.

Table 6. Viral Load Reduction in HEp-2 2D vs. EpiAirway 3D Cell Culture

RSV Strain	Log$_{10}$ Viral Load Reduction							
	GS-5806		PC786		ALS-8112		RSV-604	
	2D	3D	2D	3D	2D	3D	2D	3D
A Long	1.9 ± 1.4	1.3 ± 0.04	3 ± 0.3 (4)	2.2 ± 0.4	0.4 ± 0.3	1.2 ± 0.3	3 ± 0.3	2.4 ± 1.2
B VR-955	0.9 ± 0.9	1.1 ± 0.3 (4)	2.2 ± 0.2	1.5 ± 0.6	0.4 ± 0.3	1.4 ± 0.4	1.5 ± 0.3	2.2 ± 0.4
A2	1.8 ± 0.8	1.3 ± 0.5 (4)	3.5 ± 0.5	3.3 ± 0.3	0.7 ± 0.4	1.8 ± 0.3	3.4 ± 0.5	3 ± 0.7
CI A 121301343	2.2 ± 0.5	1.4 ± 0.8 (4)	3.4 ± 0.5	2.4 ± 0.8	1.4 ± 0.6 (4)	1.6 ± 0.4	3.6 ± 0.8	2.2 ± 0.7
CI B 65848	2.6 ± 0.9	1.2 ± 0.4	2 ± 0.8	2.1 ± 0.5	1.9 ± 0.2 (5)	1.3 ± 0.5	3.3 ± 0.6	3 ± 0.5

Table comparing log$_{10}$ viral load reduction at the point of maximum inhibition across 5 laboratory and clinical strains of RSV in HEp-2 2D cell culture and EpiAirway 3D cell culture. All treatments were given at the time of infection. N=3 for all samples except where specified by number in parentheses.

To rule out the effect of compound cytotoxicity on antiviral effect, the LDH assay was used to compare each compound treatment to untreated tissue. It was observed that GS-5806 (p<0.01), PC786 (p<0.01), RSV-604 (p<0.05), and ALS-8112 (p<0.05) resulted in a less than 1.3-log$_2$ fold higher signal than untreated tissue in the LDH cytotoxicity assay. A higher signal indicates a greater amount of LDH in the cell media, presumably due to cell destruction or death. RSV-A Long infection did not result in a significantly different signal than uninfected cells. All conditions resulted in a cytotoxicity of less than 10% (Table 7).

Table 7. Cytotoxicity in the EpiAirway Model

Treatment	N	Concentration Tested (nM)	Fold RSV-A Long EC$_{50}$	% Cytotoxicity
RSV-A Long Infection	3	NA	NA	4.5
GS-5806	5	60	24	7.1
PC786	5	50	34	6.1
ALS-8112	6	15,000	6	4.0
RSV-604	6	5,400	20	5.5

Cytotoxicity as measured in the LDH Assay using uninfected, untreated cells as a 0% cytotoxicity reference and cells killed by triton X-100 as a 100% cytotoxicity reference. Signal to background for controls was 21. Each N represents one tissue.

Specific Aim 2

The goal of this aim was to determine if delaying compound treatment or changing the delivery method would influence compound efficacy in the EpiAirway 3D culture model.

Alternate Treatment Methods

While attempting to compare basal and apical compound delivery, it was determined that apical exposure was not possible for extended treatments, as the lack of air exposure resulted in a significant visual impact on EpiAirway tissue health (Figure 18 in Appendix 2). Therefore, no experiments could be run comparing these variables.

Delaying the time of treatment delivery was possible in the EpiAirway model, and 2 time points were chosen to study the impact on efficacy. When compound treatments were applied 6 hours or 3 days after RSV-A Long infection, there was a tendency towards less viral load reduction when compared to samples given treatment at the time of infection (Figure 11). There was no evident trend observed for EC$_{50}$ changes due to delayed treatment (Table 8).

37

Table 8. Compound EC$_{50}$ with Delayed Treatment in EpiAirway Tissue

Time Compound Added (Post-infection)	RSV-A Long EC$_{50}$ (nM)		
	0h Addition	6h Addition	3d Addition
GS-5806	2.5 ± 2.3	10.4 ± 13.2	0.9
PC786	1.5 ± 0.7	0.9 ± 0.5	0.6 ± 0.4
ALS-8112	$2,492 \pm 2,109$	$1,298 \pm 705$	1,663
RSV-604	402 ± 153	143 ± 64	181 ± 98

Table showing EC$_{50}$ for compounds added to well medium 6 hours or 3 days after RSV-A Long infection, compared to EC$_{50}$ when compound is given at time of infection. Values shown as average ± standard deviation. If no standard deviation is given, viral inhibition curves did not allow for exact EC$_{50}$ determination for all replicates. N=3 for all samples.
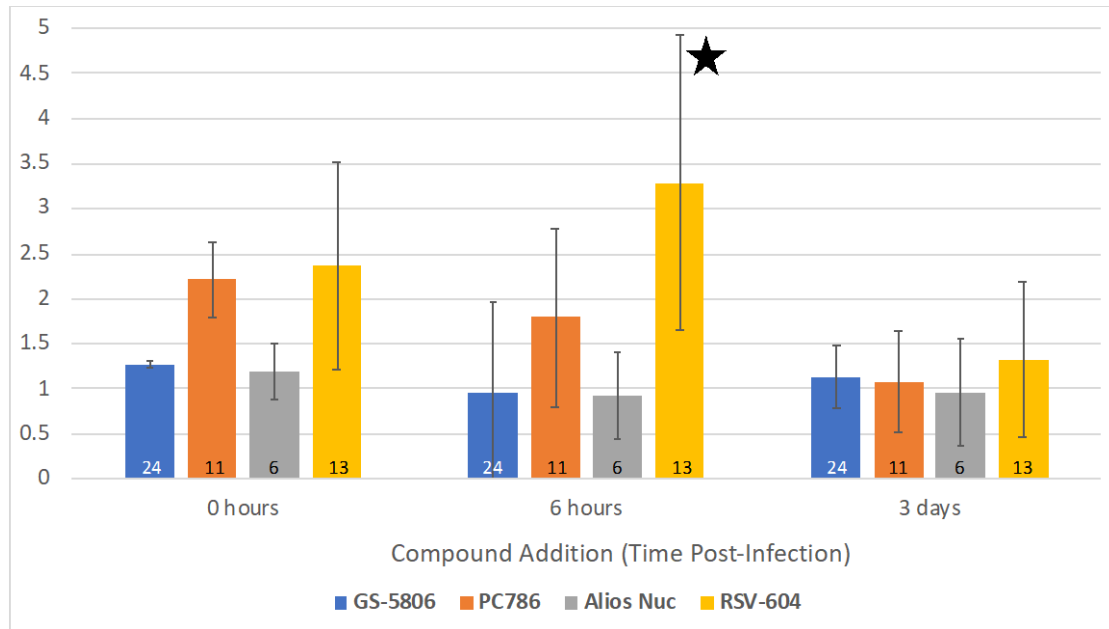
Figure 11. Average Log$_{10}$ Viral Load Reduction with Delayed Treatment

Viral load log$_{10}$ reduction at the point of greatest viral inhibition. Numbers on the bottom of each bar indicate maximum concentration the compound was tested up to, relative to fold-RSV-A Long EC$_{50}$ when compound is added at time of infection. Error bars represent standard deviation. RSV-604 treatment at 6 hours is starred, as one of the replicates had a viral load below the limit of detection. Therefore, a 4.8-log$_{10}$ reduction was included in the average despite the true value being >4.8.

Significant viral load reduction at the point of maximum inhibition was observed at endpoint for all samples where treatment was applied 6hpi or 3dpi ($p<0.01$, $p<0.05$ respectively). This was also true for average viral load when inhibition was greater than 50% for all 6hpi treatment and PC786 and RSV-604 3dpi treatment ($p<0.05$). However, 3dpi treatments at endpoint failed to reduce viral load beyond levels seen with untreated, infected tissue collected at 3dpi or 5dpi. The exception was ALS-8112 3dpi treatment, which had lower endpoint viral load at maximum inhibition than the viral load of untreated, infected tissue at 5dpi ($p<0.05$).

Specific Aim 3

The goal of this aim was to identify differences in RSV infection and compound treatment effectiveness between EpiAirway 3D culture of normal and diseased tissue.

Asthmatic Tissue

To observe any changes in RSV infection or treatment, EpiAirway tissues from an asthmatic donor were successfully infected and given compound. Treatment of RSV-A Long in asthmatic tissues at the time of infection with either PC786 ($p<0.01$), GS-5806 ($p<0.05$), RSV-604 ($p<0.01$), or ALS-8112 ($p<0.01$) reduced viral loads by 5dpi. These reductions were significant for maximum viral inhibition and average inhibition at concentrations above the EC_{50}. There was no significant difference in viral load reduction between treated asthmatic and normal tissues (Figure 12). The overall trend was for treated asthmatic tissues to have higher EC_{50}s and lower viral load reduction compared to treated normal tissues. There was no significant difference in viral load reduction between compound treatments (Table 9).

39

Table 9. Compound Efficacy in Normal vs. Asthmatic EpiAirway Tissue

Treatment	RSV-A Long EC$_{50}$ (nM)		Log$_{10}$ Viral Load Reduction	
	Normal Tissue	Asthma Tissue	Normal Tissue	Asthma Tissue
GS-5806	2.5 ± 2.3	0.6 ± 0.02	1.3 ± 0.04	0.9 ± 0.6
PC786	1.5 ± 0.7	2.9 ± 1.4	2.2 ± 0.4	1.4 ± 0.6
ALS-8112	$2,492 \pm 2,109$	$5,250 \pm 3,367$	1.2 ± 0.3	1.3 ± 0.7
RSV-604	402 ± 153	411 ± 184	2.4 ± 1.2	1.8 ± 0.4

Table showing EC$_{50}$ and log$_{10}$ viral load reduction at the point of maximum inhibition. Compounds added to cell medium at time of RSV-A Long infection in tissue from normal or asthmatic donors. Values shown as average ± standard deviation. N=3 for all samples.
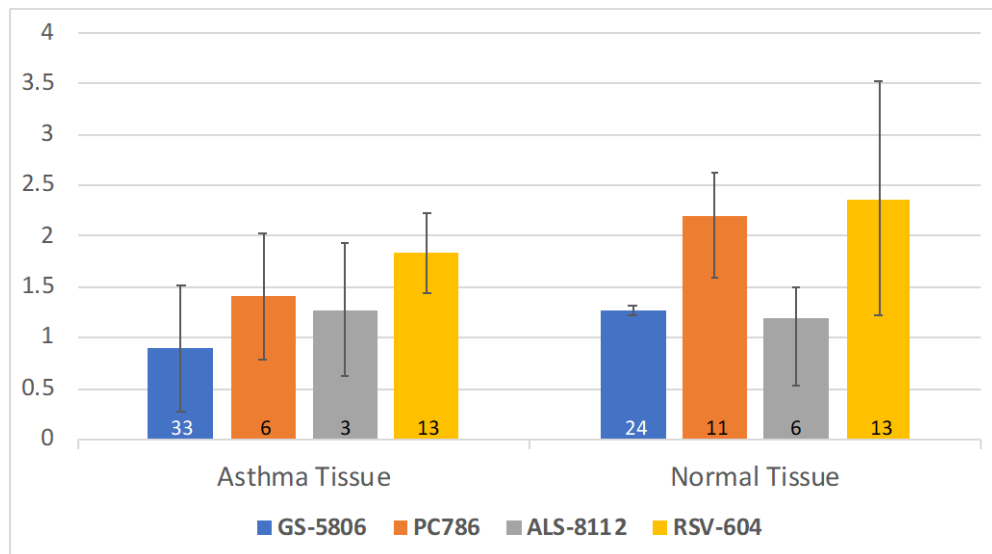
Figure 12. Average Log$_{10}$ Viral Load Reduction in Asthmatic EpiAirway Tissue

Viral load log$_{10}$ reduction at the point of maximum viral inhibition. Numbers on the bottom of each bar indicate maximum concentration the compound was tested up to, relative to fold-RSV-A Long EC$_{50}$ in normal tissue. Error bars represent standard deviation.

Cytokine Analysis

Through MSD analysis it was confirmed that cytokine concentrations could be measured in EpiAirway medium at 5dpi for normal and asthmatic tissue. Most samples did not have a measurable concentration of periostin, so no trends or significant results were found. When comparing concentrations before and after RSV-A Long infection, the overall trends were IL-6, IP-10, and RANTES increasing and IFN-α2α, IL-7, and IL-8 decreasing after infection (see Figure 13 for significance).

	Treatment, Max [] Tested (x-times EC_{50})	Fractalkine	IFN-α2α	IL-10	IL-33	IL-2	IL-6	IL-7	IL-8	IP-10	TSLP	RANTES
Normal Tissue	DMSO	NA	0.04	0.72	0.50	0.63	0.55	0.03	0.10	-0.24	0.06	0.30	-0.33
	GS-5806	24	0.19	-0.11	0.30	0.12	-0.17	0.39	-0.40	-0.25	0.90 ★	-0.22	1.53
	PC786	33	0.09	-0.52	-0.04	-0.32	-0.38	0.91	-0.84	-0.19	1.20	-0.82	1.09
	ALS-8112	6	0.09	-0.02	0.06	0.05	0.03	1.69	0.04	0.25	0.73	-0.28	2.26
	RSV-604	13	0.07	0.06	-0.31	0.07	-0.16	-0.03	0.03	-1.05	0.60	-0.17	1.63
Asthma Tissue	DMSO	NA	-0.10	-1.23	0.75	-0.25	0.06	0.89 ★	0.18	-0.44	1.02 ★	-0.07	0.41
	GS-5806	24	0.22	-0.02	0.55	0.22	0.10	0.42	-0.08	-0.41	0.67	0.24	1.47
	PC786	33	0.25	-0.41	0.10	0.03	-0.08	0.58	-0.23	-0.02	0.65	0.00	1.39
	ALS-8112	6	0.11	-0.07	0.15	0.08	0.00	0.65	-0.20	-0.57	0.22	0.39	1.42
	RSV-604	13	0.20	0.60	-0.12	1.11	-0.15	0.41	-0.17	0.41	0.49	0.49	0.36

Decreased Concentration — Increased Concentration

Figure 13. Cytokine Response to RSV-A Long Infection in EpiAirway Model

Heat map showing $\log_2$ fold shift in cytokine concentration in infected tissue using uninfected tissue as a reference. All comparisons are made within each treatment condition. Top compound concentrations listed in reference to RSV-A Long EC_{50} in normal tissue. Red stars indicate significance $p<0.05$.

For uninfected normal tissues, IFN-α2α ($p<0.05$), IL-33 ($p<0.01$), and IL-2 ($p<0.05$) increased after all compound treatment except IL-33 after PC786 treatment (Figure 14). IFN-α2α was lower in GS-5806-treated tissue than with PC786 or ALS-8112 ($p<0.05$). IL-33 was lower in GS-5806-treated samples than with RSV-604 ($p<0.01$).

Treatment	Fractalkine	IFN-α2α	IL-10	IL-33	IL-2	IL-6	IL-7	IL-8	IP-10	TSLP	RANTES
GS-5806	-0.08	1.34 ★	0.30	0.49 ★	0.85 ★	-0.34	0.61	0.21	-1.32	0.64	-1.40
PC786	0.16	1.84 ★	0.77	0.93	1.01 ★	-0.01	0.94	0.45	-0.87	0.66	-0.40
ALS-8112	-0.14	1.72 ★	0.79	0.60 ★	0.96 ★	-0.11	0.55	-0.33	-1.44	0.95	-1.36 ★
RSV-604	0.15	1.70 ★	0.72	0.73 ★	0.89 ★	0.55	0.50	-0.03	-1.47	0.54	-1.12

Decreased Concentration   Increased Concentration

Figure 14. Cytokine Shift in Uninfected Normal EpiAirway Tissue

Heat map showing log$_2$ fold shift in cytokine concentration, with each compound treatment compared to DMSO-treated samples in uninfected normal tissue. Red stars indicate significance p<0.05. Purple stars indicate significance p<0.01.

For infected normal tissues, the concentration of IFN-α2α increased and IP-10 decreased after treatment with RSV-604 (p<0.05). The concentration of IL-2 and IL-6 increased after treatment with ALS-8112 and PC786 respectively (p<0.05) (Figure 15).

Treatment	Fractalkine	IFN-α2α	IL-10	IL-33	IL-2	IL-6	IL-7	IL-8	IP-10	TSLP	RANTES
GS-5806	0.06	0.52	0.10	-0.03	0.12	0.02	0.12	0.19	-0.48	0.12	0.46
PC786	0.20	0.60	0.23	-0.02	0.07	0.87 ★	0.01	0.50	0.27	-0.46	1.02
ALS-8112	-0.09	0.98	0.36	0.02	0.43 ★	1.55	0.49	0.16	-0.77	0.36	1.23
RSV-604	0.17	1.04 ★	-0.09	0.17	0.18	0.50	0.43	-0.84	-0.92 ★	0.07	0.84

Decreased Concentration   Increased Concentration

Figure 15. Cytokine Shift in Infected Normal EpiAirway Tissue

Heat map showing log$_2$ fold shift in cytokine concentration, with each compound treatment compared to DMSO-treated samples in RSV-A Long infected normal tissue. Red stars indicate significance p<0.05.

When comparing cytokine concentrations in the differing tissue types there was an evident trend towards fractalkine, IFN-α2α, IL-10, IL-33, IL-2, IL-6, IL-7, IL-8, and IP-10 having higher concentrations in asthmatic samples than normal tissue. Conversely, concentrations of TSLP and RANTES appeared to be lower in asthmatic tissue than normal tissue (see Figure 16 for significance).

	Treatment, Max [] Tested (x-times EC_{50})		Fractalkine	IFN-α2α	IL-10	IL-33	IL-2	IL-6	IL-7	IL-8	IP-10	TSLP	RANTES
Uninfected	DMSO	NA	0.62★	2.71	0.81	1.33	1.05★	0.23	0.62	1.11★	-0.40	-1.22★	-3.82★
	GS-5806	24	0.70	0.35	0.80	0.51★	0.17	0.99	-0.04	0.94★	0.63	-2.01	-3.01
	PC786	33	0.16	0.09	0.17	0.08	-0.02	0.53	-0.11	0.38	-0.28	-1.82	-4.07
	ALS-8112	6	0.54★	0.62	0.66★	0.60★	0.18	0.49	0.42	0.98★	0.18	-2.31★	-2.97★
	RSV-604	13	0.26	1.47	1.85	2.02	0.68★	0.12	0.89	0.67	1.28	-1.69★	-2.70
RSV-A Long Infected	DMSO	NA	0.47	0.76	1.06★	0.46	0.55★	1.09★	0.70★	0.91★	0.56	-1.59★	-3.08
	GS-5806	24	0.73	0.43	1.06	0.61	0.44	1.03	0.28	0.78	0.40★	-1.55	-3.07★
	PC786	33	0.32	0.19	0.31	0.43	0.28	0.19	0.50	0.55	-0.83	-1.01★	-3.77★
	ALS-8112	6	0.56	0.57	0.74★	0.62	0.15	-0.55	0.19	0.17	-0.32	-1.64	-3.81★
	RSV-604	13	0.39	2.02	2.04	3.06	0.69	0.55	0.68	2.13	1.18	-1.02	-3.97

Decreased Concentration   Increased Concentration

Figure 16. Cytokine Response in Asthmatic EpiAirway Tissue

Heat map of $\log_2$ fold shift in cytokine concentration in asthmatic tissue with normal tissue as a reference. Top compound concentrations listed in reference to RSV-A Long EC_{50} in normal tissue. All comparisons are made within each treatment condition. Red stars indicate significance $p<0.05$. Purple stars indicate significance $p<0.01$.

In uninfected asthma tissue, fractalkine concentration was lower in PC786-treated tissue than untreated samples ($p<0.05$) (Figure 17). Concentration of IL-2 was higher in RSV-604-treated samples than with ALS-8112 ($p<0.05$), and IL-8 concentration was higher in GS-5806-treated tissue than with ALS-8112.

Treatment	Fractalkine	IFN-α2a	IL-10	IL-33	IL-2	IL-6	IL-7	IL-8	IP-10	TSLP	RANTES
GS-5806	0.00	-1.02	0.30	-0.33	-0.03	0.42	-0.05	0.03	-0.30	-0.14	-0.59
PC786	-0.30★	-0.78	0.13	-0.33	-0.07	0.28	0.21	-0.27	-0.75	0.06	-0.65
ALS-8112	-0.22	-0.37	0.64	-0.14	0.09	0.14	0.35	-0.45	-0.86	-0.15	-0.50
RSV-604	-0.21	0.46	1.77	1.41	0.52	0.44	0.77	-0.47	0.22	0.07	0.00

Decreased Concentration   Increased Concentration

Figure 17. Cytokine Shift in Uninfected Asthmatic EpiAirway Tissue

Heat map showing log$_2$ fold shift in cytokine concentration, with each compound treatment compared to DMSO-treated samples in uninfected asthmatic tissue. Red stars indicate significance $p<0.05$.

In infected asthma tissue, concentration of IFN-α2α was higher and concentration of IL-8 and IP-10 was lower after ALS-8112 treatment compared to no treatment ($p<0.05$, $p<0.05$, $p<0.01$ respectively). IP-10 concentration was also lower after PC786 treatment compared to untreated samples ($p<0.05$) (Figure 18). IP-10 concentration was lower in ALS-8112-treated tissue than with GS-5806 treatment ($p<0.01$).

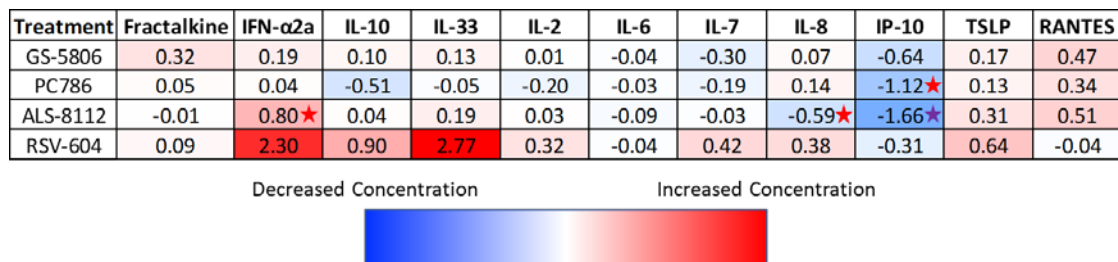| Treatment	Fractalkine	IFN-α2a	IL-10	IL-33	IL-2	IL-6	IL-7	IL-8	IP-10	TSLP	RANTES
GS-5806	0.32	0.19	0.10	0.13	0.01	-0.04	-0.30	0.07	-0.64	0.17	0.47
PC786	0.05	0.04	-0.51	-0.05	-0.20	-0.03	-0.19	0.14	-1.12★	0.13	0.34
ALS-8112	-0.01	0.80★	0.04	0.19	0.03	-0.09	-0.03	-0.59★	-1.66★	0.31	0.51
RSV-604	0.09	2.30	0.90	2.77	0.32	-0.04	0.42	0.38	-0.31	0.64	-0.04

Decreased Concentration   Increased Concentration

Figure 18. Cytokine Shift in Infected Asthmatic EpiAirway Tissue

Heat map showing log$_2$ fold shift in cytokine concentration, with each compound treatment compared to DMSO-treated samples in RSV-A Long infected asthmatic tissue. Red stars indicate significance $p<0.05$. Purple stars indicate significance $p<0.01$.

Chapter IV.

Discussion

This study provided an extensive analysis of the ability of the EpiAirway model to support RSV infection, testing multiple laboratory and clinical strains for comparison. Three analysis endpoints were established as successful measures of the EpiAirway culture environment; RNA viral load, live virus (plaque assay), and cytokine concentration. In addition, compounds with varying mechanisms of action were assessed alongside one another to examine the effect of 3 different treatment times relative to infection. Two versions of the model were studied; verifying the infection and analysis of tissues sourced from both normal and asthmatic donors. Results from this study confirm and expand upon the functions of the EpiAirway 3D model, offering up multiple avenues for further understanding of the RSV infection process and compound testing.

HEp-2 2D Culture

The EC_{50} results of PC786 and GS-5806 in HEp-2 culture were similar when tested against RSV-A strains while PC786 loses efficacy against RSV-B strains, a trend seen in published literature (Coates et al., 2017). The RSV-604 EC_{50}s ranged higher than published results in plaque reduction assays, but closer to published values seen in CPE assays as well as unpublished work at Enanta Pharmaceuticals (Chapman et al., 2007) (Perron et al., 2015). Similarly, ALS-8112 treatment resulted in EC_{50}s higher than

published results of CPE and qPCR assays, though closer to values in unpublished work at Enanta Pharmaceuticals (Coates et al., 2017) (Mirabelli et al., 2018).

EpiAirway as a 3D Model for RSV

Infection and Compound Treatment

Viral infection of EpiAirway tissue did not yield any visual CPE (Figure 17 in Appendix 2), unlike the namesake syncytia seen with RSV infection in traditional 2D cell culture (Figure 16 in Appendix 2). This is an example of 3D culture similarity to the *in vivo* environment, which also does not display the syncytia seen in 2D *in vitro* infection.

The plaque assay demonstrated that apical washes of the EpiAirway tissue could be used to measure live virus, and that PFUs increased over the course of a 10-day infection. There was a large standard deviation, as this collection process is inherently prone to variation. Washing the tissue every day may artificially increase or decrease the next day's viral collection due to factors such as cell damage from pipetting. Although this may be an imperfect method of measuring live virus, the EpiAirway model demonstrated successful tracking of viable virus production.

While the LDH cytotoxicity assay did demonstrate a difference between untreated and compound-treated tissue, the very small fold change of 1.3-log_2 suggests this difference may be biologically irrelevant. This combined with the fact that the highest concentration of all compounds tested was below the 10% cytotoxic concentration (CC_{10}) point (Table 7) indicates that any potential cytotoxicity is unlikely to account for the extent of viral load reduction that occurs with compound treatment. Since there was also no significant difference in LDH signal between infected and uninfected samples, this

assay or the EpiAirway model itself may not be suited for studies involving RSV-related CPE.

Infection experiments in the EpiAirway model demonstrate that this 3D cell culture model can be successfully utilized for study with both laboratory and clinical strains of RSV. Across the viral strains tested, the peak viral load reduction often occurred at the highest compound concentration tested, usually a spike up from the previous point. This may indicate that the maximum potential of viral load reduction was not always reached under assay conditions, and that higher compound concentrations could be pursued with this model given that they were below the 50% cytotoxic concentration (CC_{50}) value. This especially may be the case with ALS-8112 treatment against RSV-A Long tested at a concentration 6 times EC_{50}; it is possible increasing this to at least 10 times EC_{50} could yield improved reduction.

Treatment with RSV-604 and PC786 consistently demonstrated greater reduction of viral RNA compared to GS-5806 and ALS-8112 at assay endpoint across RSV-A and -B strains tested. While the fold-EC_{50} value for each compound's maximum concentration varied due to the internal comparison within each virus, it does not appear that any discrepancies between fold difference can account for the differences seen in viral load reduction. For example, despite GS-5608 being tested at a higher fold EC_{50} than RSV-604, treatment across viral strains reduced viral load by approximately 1-$\log_{10}$ while RSV-604 reduced viral load by 2- to 3-$\log_{10}$. Therefore, observed differences in viral load reduction are likely due to unique properties of individual compounds and/or to their respective mechanism of action.

Alternate Compound Treatment

Testing compound delivery on the apical side of the tissue was not possible due to the need for air exposure, therefore the EpiAirway model may not be ideal for studies seeking to emulate compound delivery through inhalation without changes to the protocol. It was decided after studies were complete to test GS-5806 treatment delivered apically along with the virus during the period of infection, to see if this would improve the low levels of viral load reduction. This approach takes into account that compound diffusion to the cell surface would likely be faster from the apical side rather than the basal, and would benefit the fusion inhibitor's mechanism of action. This initial test demonstrated a 2-log_{10} reduction in viral load at endpoint when compound was added apically and basally, compared to the 1-log_{10} reduction seen with basal treatment alone (data not shown). This suggests that adding compound apically during infection may increase the compound's effectiveness in this model. However, this process does not mimic the compound delivery of GS-5806 in actual patients, and whether this effect is limited to fusion inhibitors alone or other mechanisms of action would require further experimentation.

For RSV-A Long infected tissues, viral load measured via qRT-PCR was found to increase when 3dpi, 5dpi, and 8dpi tissue extractions were compared (3dpi<5dpi<8dpi). When samples received compound 3dpi, viral load at the 8dpi endpoint was not significantly different from untreated 3dpi or 5dpi levels but was significantly reduced compared to untreated 8dpi viral loads. This indicates that 3 day-delayed treatment maintains a 3dpi detectable viral load by the 8dpi endpoint, while still having an antiviral effect on replication compared to untreated samples. It is unknown to what degree

detectable viral load produced after addition of compound is viable, and this will be tested in future studies using a plaque assay.

Contrary to prediction, GS-5806 did not have the greatest loss of efficacy when compound treatment was delayed. Instead, the trends suggest that PC786 and RSV-604 suffered the greatest shifts in antiviral activity when delivered 3dpi. However, this could be a result of them having the largest viral load reduction to begin with, enabling any shift to appear more dramatic. With 6hpi delivery, RSV-604 had the greatest viral load reduction compared to all other compound treatments.

Comparison to published results

Observing viable virus production via a plaque assay showed an increase in PFU through 10dpi, which differs from published results in some studies which have observed the virus peaking at days 3-4 post infection (Coates et al., 2017) (D. W. Brookes et al., 2018). Reasons for this discrepancy may include differences in the 3D model used, viral strain (RSV-A2 vs. A Long), viral inoculum, or collection and plaque assay methods. In contrast, other studies show similar trends to this project, with apical wash viral load measured by qPCR increasing through 15 days post-infection (Mirabelli et al., 2018).

The EC_{50}s of GS-5806, PC786, and ALS-8112 in 3D culture were in line with published results, while the RSV-604 value was about 5.5 times lower (Perron et al., 2015) (Coates et al., 2017) (Deval et al., 2015) (Chapman et al., 2007).

When compounds were added 3dpi, ALS-8112 and PC786 treatment resulted in a smaller viral load reduction (less than 1-$\log_{10}$ and 1.1-$\log_{10}$ respectively) than seen in the Mirabelli et al. study (2-$\log_{10}$ and 3-$\log_{10}$ respectively). Treatment 3dpi with GS-5806 resulted in a greater viral load reduction than in the Mirabelli study (1.1-$\log_{10}$ versus no

antiviral effect). However, Mirabelli et al. measured viral load from apical washes rather than the tissue itself, had an endpoint of 7dpi, and tested compounds at a minimum of 100 times the EC_{50}, higher than tested in this project (Mirabelli et al., 2018). As previously stated, increasing drug concentration may improve viral load reduction. In a study by Brookes et al., the EC_{50}s of PC786 (apical application) and ALS-8112 (basolateral application) when added 3dpi were higher than the values seen in this project (256 times and 9.3 times higher respectively). However, the viral inoculum, treatment and measurement methods, and drug concentrations differed once again from the methods used in this project (D. W. Brookes et al., 2018).

Asthmatic Tissue in the 3D Model

When comparing the 5-day assay in both normal and asthmatic tissues there was no difference in viral load, indicating that any distinction between donor tissue in this model did not negatively or positively impact RSV infection. This is in-line with the study by Bai et al. in a 3D model where there was no significant difference in viral load found between asthmatic and non-asthmatic tissues when infected with RV-A16 (human rhinovirus A16) (Bai et al., 2015). Trends in compound EC_{50} and viral load reduction suggest that compound efficacy is negatively impacted in asthmatic tissue, in line with prediction and published values (Deval et al., 2015). It is not clear from the experiments run in this study which aspects of the asthmatic donor tissue may impact compound efficacy, if these trends would be seen in actual patients, or if there is any relation to the more severe RSV symptoms seen in asthma patients. It is also possible that decreased compound efficacy would be even more evident *in vivo*. While some data were eliminated during this analysis as outliers, more recent data calls this into question.

However, these data remain excluded, as more points are needed to confirm or deny their outlier status.

Comparison to the 2D Culture Model

Data from the 2D and 3D cell culture models cannot be directly compared, as there are extensive differences between the two methods and the cell type is drastically different. However, 2D culture with HEp-2 cells is accepted as the industry standard for studying RSV infection and treatment. Having these values allows comparison with external studies as well as between strains within each culture method; and may offer insight as to differences between 2D and 3D culture performance. The 3D EpiAirway model allows for infection over a longer period of time without loss of viral load (tested up to 10 days in this project), which is superior over 2D culture for experiments requiring multiple time points. In contrast, HEp-2 2D culture cannot last much longer than 5 days post-RSV infection, even with a low MOI of 0.01.

Contrary to prediction, viral loads of RSV-A and -B strains tested were not significantly different at assay endpoint in untreated 2D culture extractions compared to untreated 3D culture extractions. It cannot be concluded that one model is superior for studying RSV infection from these results, though it does suggest that viral infection may proceed similarly in both models. However, there are many differences between 2D and 3D culture that must be taken into account. Such factors include but are not limited to the fact that the 2D model does not have the inoculum washed away after 1 hour nor compound replaced during the experiment, whereas the 3D model requires inoculum to be washed off after 1 hour and compound replaced every 2-3 days. One of the major differences is that the 2D culture is composed of cancerous cervical cancer cells and the

3D tissues are comprised of primary cells from patient tracheal and bronchial tissue, which most likely results in differing infection and cell division rates. Another unavoidable distinction is that infection of the 2D model is done with a MOI of 0.1 based on cell count, while infection of the 3D model is based on a consistent amount of PFU per well representing an estimated 0.1 MOI.

Based on EC_{50}, compounds tended to perform best against RSV-A2 in 3D culture, while in 2D cell culture the compounds tended to perform best against RSV-B clinical isolate 65848 (Table 5). With regards to differences between RSV-A and RSV-B strains, only PC786 treatment demonstrated decreased performance in the RSV-B subtype compared to RSV-A, seen in both 2D and 3D cell culture. In the 2D model, GS-5806 had the lowest EC_{50} across all viruses tested. In the 3D model, both PC786 and GS-5806 treatment trended this way (Table 5). Based on viral load reduction, both cell culture models displayed the same trends with regards to compound effectiveness; treatment with PC786 or RSV-604 consistently demonstrated greater reduction in viral load compared to treatment with GS-5806 or ALS-8112. GS-5806 treatment reached a viral load reduction of over 2-log_{10} in 2D culture but is around 1-log_{10} in 3D culture against the RSV clinical isolates tested (Table 6). With regards to a 5-day assay, the data supports 2D and 3D cell culture models giving comparable results with regards to compound effectiveness. It may be useful for future studies to compare time-of-addition assays in both 2D and 3D culture to see if a significant difference exists with regards to reduction of viral load and/or EC_{50}.

Contrary to prediction, the compound EC_{50} trend was lower values in the 3D culture model than in the 2D culture model, with the exception of GS-5806 which had the reverse trend for several conditions. Once again, due to the differences between models it

cannot be concluded if this is due to decreased viral replication. Factors that may be influencing this trend in addition to the model differences discussed above are the compounds' respective mechanism of action and/or stability, interaction and binding with proteins, and timing required for the compound to diffuse through the basal-side tissue as the virus is exposed to the apical-side tissue.

Limitations of the 3D Culture Model

Due to the nature of this model, there are some factors which remain variable across donors and potentially across tissue lots. Since the 3D cell culture plates are received from an external source, with cell collection and seeding done by another individual, exact details of the materials received cannot be known. For example, the precise number of cells in each well and the cell composition of each tissue by the time it arrives for use in this study is estimated based on an average given by the vendor. There will be variability due to individual cell growth that cannot be accounted for. If the ratio of goblet to basal cells impacts infection and differs significantly between all plates or specifically between normal and diseased tissues, this could affect the degree to which tissues can be infected and how antiviral treatments perform. Any correlation of experimental outcome to real world clinical results is beyond the scope of this project.

Maximum compound concentration tested was limited by solubility factors and the need to keep the DMSO concentration below 0.1%, which especially impacted ALS-8112 treatment as it had the highest EC_{50} of the compounds tested.

Cytokines in the EpiAirway Model

As expected, over half of treatment conditions in both normal and asthmatic tissue resulted in an increase in cytokine concentration after infection with RSV-A Long. The degree of change was varied, with RANTES, IP-10, and IL-6 having some of the greatest increases. RANTES may have been increasing in the process of reaching peak levels after day 5. These results are in agreement with published observations of these cytokines increasing after RSV-A2 infection (D. Brookes et al., 2016). The one exception was IL-8 concentration, which decreased after infection despite having a correlation with more severe disease. Release of IL-8 has been shown to increase after infection of A549 cells in 2D culture with RSV (McAllister et al., 2020), and even more so after infection with rhinovirus, through 2dpi (Chun et al., 2013). It is possible that IL-8 release decreases after this 2-day point, and the 3D model media change at 2 days post-infection results in the cytokine level being lower in the infected tissues compared to the uninfected tissues where IL-8 release has not changed. Or the majority of increase has occurred by two days, and any remaining amount produced after the media change is not sufficient to register as an increase. Another approach could be that one of the other cytokines down-regulates the release of IL-8 under the 3D culture conditions, or that factors outside those available in the EpiAirway model favor an increase in IL-8 over a decrease. IL-7 and IFNα2α also displayed a more subtle decrease, the latter being in line with mouse *in vivo* results showing poor induction of IFN-α by RSV (Guerrero-Plata et al., 2005).

As expected, the majority of cytokines had higher concentrations in asthmatic tissue than normal tissue, regardless of infection status. It is possible that this result is due to carryover from an increased inflammation status in asthma patients that is maintained

in the EpiAirway model. Strong exceptions were TSLP and RANTES, which were lower in asthmatic tissues across all conditions.

The difference in TSLP and RANTES levels between normal and asthmatic samples was the reverse of published data (Ying et al., 2005) (Rojas-Ramos et al., 2003), which could be for multiple reasons. It is possible that since pooled donors were not used, the specific donors for each condition may have been on the extreme end of cytokine concentration levels by chance. The expected higher levels of TSLP and RANTES may only occur in asthma patients *in vivo*, requiring factors external to cell culture for levels to increase despite being known to be released from epithelial cells. TSLP signaling plays a strong role in airway inflammation, so its lower concentration in EpiAirway tissue from an asthmatic donor compared to normal tissue bears further interrogation.

One of the factors that likely contributed to the minimal significant results seen in the cytokine analysis is the lack of immune cells in the EpiAirway 3D model. There are many interactions between different cell types that can influence the up- or down-regulation of cytokine release which would not be replicated in the EpiAirway model. It is also possible that by collecting basal media at 5dpi, there is the potential of losing information from cytokine levels before the 2dpi media change. Some cytokine levels may also peak earlier or later than the 5dpi timepoint at which samples were collected. In addition, it is very likely that any compound-related cytokine results may require a higher concentration than those tested in this study. Furthermore, any comparison to DMSO-treated samples would be influenced if the reference samples resulted in atypical or false changes in cytokine concentration. At this point, there is insufficient data to confirm any individual compound-specific effects on cytokine concentration. The analysis for this

project only represents a snapshot of the cytokines present in well medium at a specific point, and therefore any biological relevance extrapolated from these results must be made with this limitation in mind.

Future 3D Model Studies

For experiments with alternate infection methods, factors such as increasing the MOI used for infection or the length of viral incubation may impact compound efficacy. For future studies with the EpiAirway model, it would be beneficial to use multiple analytical techniques over a time course of infection. One major goal would be to determine which day post-infection that peak viral load occurs with different strains of RSV, utilizing both qRT-PCR and plaque assays to determine total and live virus present. The plaque assay is crucial to elucidate whether the PCR signal measured at the experimental endpoint is due to live virus rather than dead RNA. This is especially applicable for time-of-addition studies, wherein viral load reduction was seen at assay endpoint but not beyond levels seen with untreated, infected tissue 3 and 5dpi. Knowing how much of the RNA present in the culture represents viable, infectious virus could significantly change how the results are interpreted. For example, compound treatment delivered at specific timeframes relative to infection may result in the production of non-viable virus. If this is the case, a qRT-PCR readout would be insufficient to pick up on this antiviral effect due to the presence of RNA. Running plaque assays on samples collected before and after compound treatment in addition to the endpoint will be run in future experiments.

A time course could be utilized with regards to cytokine analysis, to see if any cytokines peak at different days post-infection. Also, time-of-compound-addition studies

could be done in more detail, including more time points and comparison with 2D cell culture studies of the same type. Measuring viral rebound after ceasing compound treatment would be a valuable endpoint to explore in this context. Western blot analysis would be another useful method of examining viral or target protein levels over the course of an infection, as a result of treatment, or between different RSV strains. This can further be related to mechanism of action by tracking a compound's target protein over the course of RSV infection and treatment.

To approximate inhaled compound delivery, several alterations would have to be made to the protocols used in this project. As suggested earlier, GS-5806 showed improved efficacy when given basally throughout infection and apically during the 1-hour viral incubation. Another follow-up step would be to test if compounds meant for inhaled delivery can have an antiviral effect solely from apical treatment in this model. The first step of this experiment would be to optimize how many apical treatments to give per day and how long the compound would be left on the tissue surface each time before aspiration.

Gene expression analysis would be an interesting approach to see if any pathways are up- or down-regulated in infected or asthmatic EpiAirway tissue. In particular, the MUC5AC gene and/or Mucin 5AC protein expression would be a beneficial target, to observe the extent of RSV-induced exacerbation of mucus production and if this is worsened in asthmatic tissue. This is especially relevant since increased mucus can contribute to more severe RSV symptoms, and antiviral compounds which reduce mucus production may be very beneficial for patient hospitalization risk (Stier et al., 2016). This target has precedent, as Mucin 5AC protein has been measured in high levels in

uninfected A549 cells but decreased after RSV infection due to cell death. There is no MUC5AC response in HBECs grown in 2D culture, but primary bronchial epithelial cells in 3D culture were shown to have slightly increased gene expression and varied protein levels after infection (McAllister et al., 2020). Expression analysis may also be an improved approach to study periostin levels in the 3D model, since MSD assays did not yield detectable concentration.

Another path of experimentation would be to use viral strains that have developed compound-resistant mutations from passage in the presence of compound in 2D cell culture. It would be interesting to see if these viruses maintain resistance in the 3D model, and if viral fitness impacts infection.

For further disease studies, alternate donors could be studied, such as tissue from COPD patients, which is another disease closely associated with severe RSV. Also, additional asthma donors could be studied to determine if the trends seen in this study hold true for other asthmatic donor tissues.

The EpiAirway model used in this project lacks immune cells, which limits the extent of cytokine and viral studies – particularly when comparing normal and diseased donor tissue response to infection. There is an alternative version of this 3D model from MatTek with stromal fibroblast cells (EpiAirwayFT) that would be interesting to explore these same experiments through the lens of inflammation.

Conclusion

The EpiAirway 3D cell culture model was successfully used to study infection and compound treatment of 5 strains of RSV. Viral load was detectable through 10dpi, and a significant decrease in viral load was evident when antiviral compounds were

applied to the culture medium. Differences between treatments were measurable using qRT-PCR and gave results comparable to trends seen in 2D cell culture. A tendency towards decreasing efficacy could be seen when compound administration was delayed following RSV infection. The tissues continued to survive without significant CPE at least 10dpi, indicating the model has potential for extended time-of-compound-addition studies. Although limited significance was seen, studies with asthma donor tissue suggest that this model may be useful for studying differences in infection, cytokine response, and treatment in normal versus disease conditions. With greater flexibility and increased options for infection studies as well as a more realistic cell scaffold, the EpiAirway tissues are an excellent model for the study of Respiratory Syncytial Virus.

Appendix 1.

Supplemental Data

Included in this appendix are additional data tables to more fully understand the methods and conclusions throughout this project.

Table 10. Compound Efficacy in Normal EpiAirway Tissue 6hpi

Treatment	EC_{50} (nM)	EC_{90} (nM)	Log_{10} Viral Load Reduction
GS-5806	10.4 ± 13.2	NA*	0.96 ± 0.99
PC786	0.9 ± 0.5	2.8 ± 2.9	1.8 ± 1
ALS-8112	$1,298 \pm 705$	$1,989$	0.9 ± 0.5
RSV-604	143 ± 64	347 ± 235	2.5 ± 1.4

*Table showing compound efficacy with respect to EC_{50}, EC_{90}, and log_{10} viral load reduction, the latter using the point of maximum viral inhibition as reference, when treatment is delayed by 6 hours. Values are displayed as average ± standard deviation. *Exact value not available due to limited curve.*

Table 11. Compound Efficacy in Normal EpiAirway Tissue 3dpi

Treatment	EC_{50} (nM)	EC_{90} (nM)	Log_{10} Viral Load Reduction
GS-5806	0.9	NA*	1.1 ± 0.4
PC786	0.6 ± 0.4	0.7 ± 0.04	1.1 ± 0.6
ALS-8112	$1,663$	$4,250 \pm 736$	0.96 ± 0.6
RSV-604	181 ± 98	$847 \pm 1,082$	1.3 ± 0.9

*Table showing compound efficacy with respect to EC_{50}, EC_{90}, and log_{10} viral load reduction, the latter using the point of maximum viral inhibition as reference, when treatment is delayed by 3 days. Values are displayed as average ± standard deviation. *Exact value not available due to indeterminate curve.*

Table 12. Compound Efficacy in Asthmatic EpiAirway Tissue

Treatment	EC$_{50}$ (nM)	EC$_{90}$ (nM)	Log$_{10}$ Viral Load Reduction
GS-5806	0.6 ± 0.02	NA*	0.9 ± 0.6
PC786	2.9 ± 1.4	3.6 ± 2.4	1.4 ± 0.6
ALS-8112	$5,250 \pm 3,367$	$11,230$	1.3 ± 0.7
RSV-604	411 ± 184	499 ± 125	1.8 ± 0.4

*Table showing compound efficacy with respect to EC$_{50}$, EC$_{90}$, and log$_{10}$ viral load reduction, the latter using the point of maximum viral inhibition as reference. All treatments given at the time of RSV-A Long infection. Values are displayed as average ± standard deviation. *Exact value not available due to limited curve.*

Table 13. Cytokine Concentration in Normal EpiAirway Tissue

Condition	Concentration (pg/mL)										
	Fractalkine	IFN-α2α	IL-10	IL-33	IL-2	IL-6	IL-7	IL-8	IP-10	TSLP	RANTES (fg/mL)
Uninfected, Untreated	962 ± 12	2 ± 1	0.2 ± 0.1	0.7 ± 0.1	2 ± 0.9	12 ± 7	10 ± 4	$3,592 \pm 73$	60 ± 29	28 ± 10	9 ± 3
Infected, Untreated	991 ± 398	3 ± 1	0.3 ± 0.1	1 ± 0.3	3 ± 0.7	12 ± 7	11 ± 4	$3,049 \pm 1,350$	63 ± 17	34 ± 5	7 ± 4
Uninfected, GS-5806	909 ± 128	4 ± 0.6	0.3 ± 0.02	0.9 ± 0.03	4 ± 0.4	10 ± 6	16 ± 4	$4,144 \pm 1,203$	24 ± 1	43 ± 20	3 ± 3
Infected, GS-5806	$1,034 \pm 92$	4 ± 2	0.4 ± 0.2	1 ± 0.1	3 ± 0.9	13 ± 9	12 ± 7	$3,482 \pm 726$	45 ± 13	37 ± 23	9 ± 6
Uninfected, PC786	$1,071 \pm 331$	6 ± 0.7	0.4 ± 0.1	1 ± 0.4	4 ± 0.5	12 ± 5	20 ± 6	$4,913 \pm 1,670$	33 ± 12	44 ± 22	7 ± 6
Infected, PC786	$1,138 \pm 189$	4 ± 3	0.4 ± 0.1	1 ± 0.4	3 ± 1	23 ± 4	11 ± 3	$4,315 \pm 1,147$	76 ± 50	25 ± 10	14 ± 8
Uninfected, ALS-8221	870 ± 104	5 ± 0.4	0.4 ± 0.1	1 ± 0.1	4 ± 0.4	11 ± 8	15 ± 4	$2,863 \pm 692$	22 ± 3	53 ± 16	3 ± 1
Infected, ALS-8221	928 ± 288	5 ± 2	0.4 ± 0.1	1 ± 0.3	4 ± 0.4	37 ± 42	15 ± 3	$3,396 \pm 1,016$	37 ± 16	44 ± 24	16 ± 12
Uninfected, RSV-604	$1,065 \pm 622$	5 ± 0.8	0.4 ± 0.1	1 ± 0.04	4 ± 0.8	18 ± 15	14 ± 5	$3,518 \pm 1,304$	22 ± 5	40 ± 10	4 ± 4
Infected, RSV-604	$1,116 \pm 216$	6 ± 2	0.3 ± 0.04	1 ± 0.4	3 ± 0.7	18 ± 11	15 ± 2	$1,699 \pm 1,485$	33 ± 9	36 ± 23	12 ± 15

Cytokine concentration as detected in normal EpiAirway tissue, either uninfected or infected with RSV-A Long. All compound treatments, if given, were applied at time of infection.

Table 14. Cytokine Concentration in Asthmatic EpiAirway Tissue

Condition	Concentration (pg/mL)										
	Fractalkine	IFN-α2α	IL-10	IL-33	IL-2	IL-6	IL-7	IL-8	IP-10	TSLP	RANTES (fg/mL)
Uninfected, Untreated	1,476 ± 213	11 ± 11	0.4 ± 0.2	2 ± 0.8	4 ± 2	14 ± 6	16 ± 4	7,753 ± 1,905	46 ± 21	12 ± 3	0.6 ± 0.4
Infected, Untreated	1,376 ± 85	5 ± 2	0.7 ± 0.2	1 ± 0.4	4 ± 1	27 ± 13	18 ± 3	5,721 ± 1,903	93 ± 42	11 ± 2	0.8 ± 0.4
Uninfected, GS-5806	1,478 ± 492	5 ± 4	0.5 ± 0.2	1 ± 0	4 ± 1	19 ± 11	15 ± 0.3	7,935 ± 542	37 ± 24	11 ± 0.9	0.4 ± 0.1
Infected, GS-5806	1,719 ± 309	5 ± 3	0.8 ± 0.3	2 ± 0.4	4 ± 1	26 ± 21	14 ± 2	5,985 ± 1,854	59 ± 4	13 ± 1	1 ± 0.8
Uninfected, PC786	1,196 ± 76	6 ± 4	0.5 ± 0.3	1 ± 0.5	4 ± 1	17 ± 7	18 ± 4	6,410 ± 2,250	27 ± 7	12 ± 3	0.4 ± 0.1
Infected, PC786	1,426 ± 355	5 ± 3	0.5 ± 0.2	1 ± 0.4	4 ± 1	26 ± 12	16 ± 5	6,300 ± 4,203	43 ± 13	12 ± 3	1 ± 0.6
Uninfected, ALS-8221	1,268 ± 65	8 ± 2	0.7 ± 0.1	2 ± 0.2	5 ± 0.3	16 ± 6	20 ± 6	5,663 ± 1,052	25 ± 7	11 ± 1	0.4 ± 0.4
Infected, ALS-8221	1,366 ± 215	8 ± 1	0.7 ± 0.1	2 ± 0.4	4 ± 1	25 ± 13	17 ± 1	3,808 ± 680	29 ± 2	14 ± 3	1 ± 0.9
Uninfected, RSV-604	1,273 ± 193	15 ± 7	1 ± 0.9	4 ± 2	6 ± 0.5	19 ± 7	27 ± 9	5,612 ± 2,600	53 ± 32	13 ± 5	0.6 ± 0.6
Infected, RSV-604	1,462 ± 216	22 ± 21	1 ± 0.9	10 ± 9	5 ± 2	26 ± 22	24 ± 17	7,458 ± 3,912	75 ± 32	18 ± 10	0.8 ± 0.7

Cytokine concentration as detected in EpiAirway tissue from the asthmatic donor, either uninfected or infected with RSV-A Long. All compound treatments, if given, were applied at time of infection.

Appendix 2.

Supplemental Figures

Included in this appendix are additional figures and graphics to more fully understand the methods and conclusions throughout this project. Photos of the EpiAirway tissue have a red color when taken in the hanging top plate due to the 5 mL of media present in the wells.
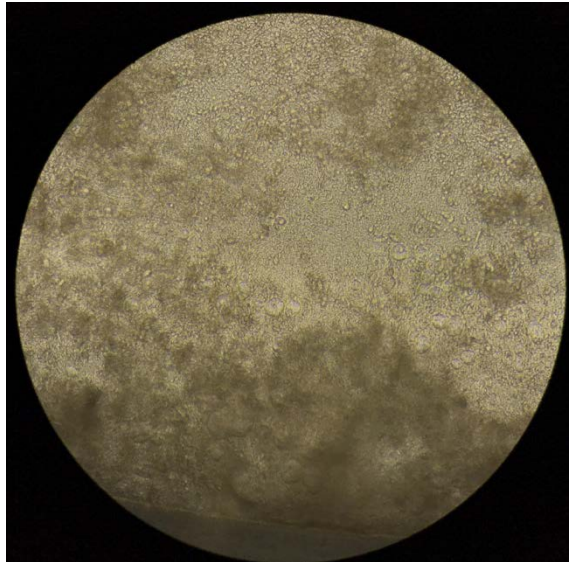

Figure 15. EpiAirway Tissue Post-equilibration

Taken at 40x magnification using Revolve Pro camera software on an inverted microscope. The dark area of the view field displays the mucus present on the apical side of the tissue. This mucus is washed off with 400 μL of TEER buffer before infection and every 7 days during cell culture.
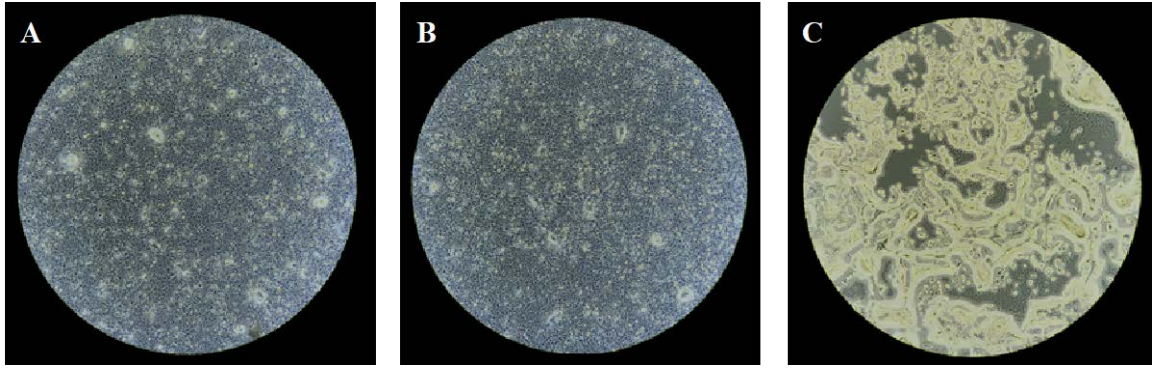
Figure 16. HEp-2 2D Culture

Taken at 40x magnification using Revolve Pro camera software on an inverted microscope. Panel A shows uninfected HEp-2 cells, panel B shows HEp-2 cells infected with RSV-A Long at a MOI of 3 and treated with 100nM PC786, panel C shows HEp-2 cells infected with RSV-A Long at a MOI of 3. Images were taken 48hpi with supernatant removed.
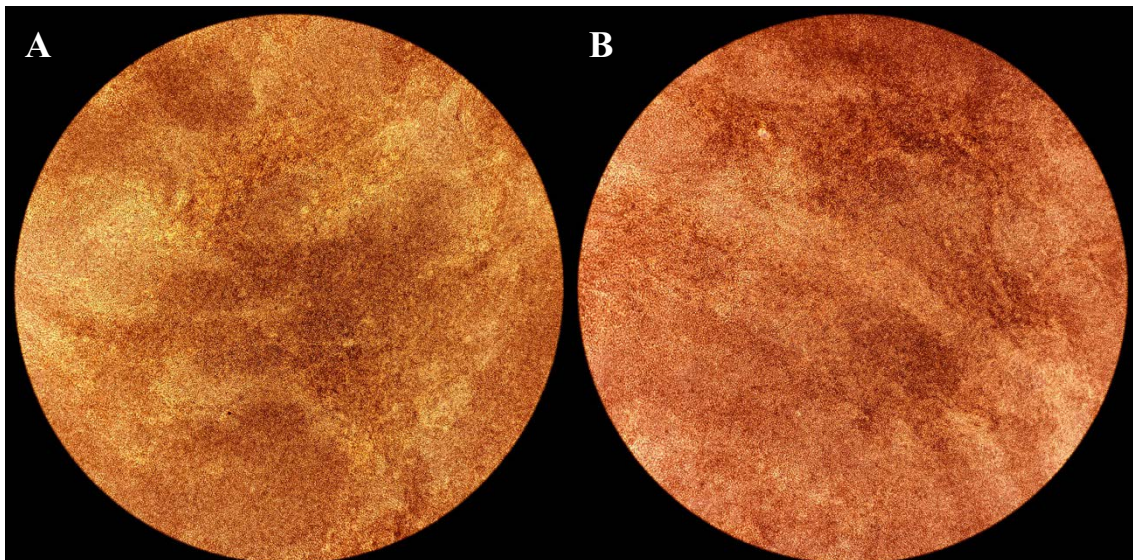

Figure 17. EpiAirway Tissue Infection

Taken at 40x magnification using Revolve Pro camera software on an inverted microscope. Panel A shows uninfected EpiAirway Tissue and panel B shows tissue infected with RSV-A Long. Both images were taken 5dpi.
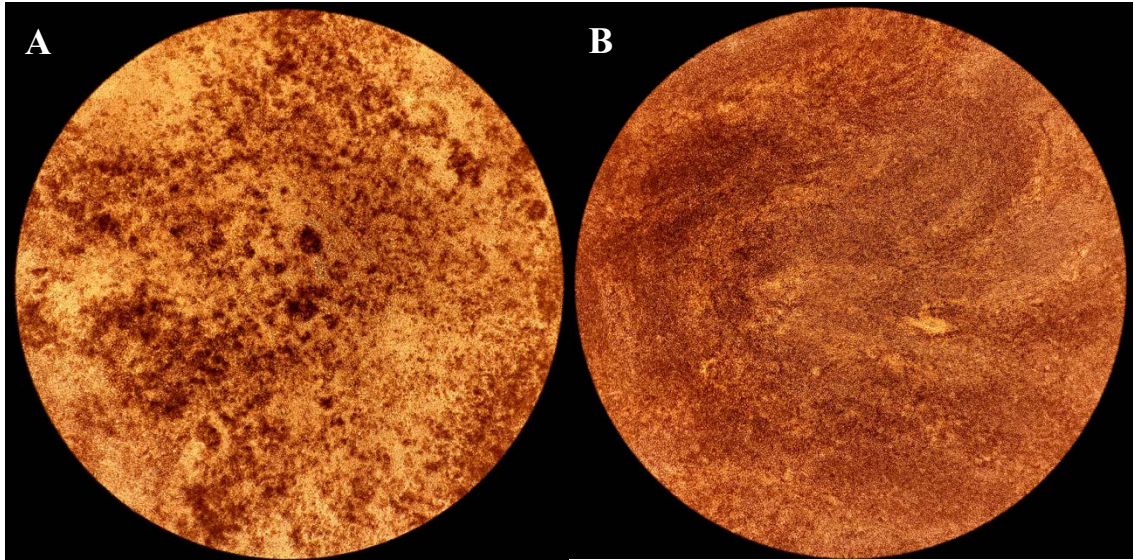
Figure 18. EpiAirway Tissue Compound Treatment

Taken at 40x magnification using Revolve Pro camera software on an inverted microscope. Panel A shows infected tissue treated with PC786 apically and panel B shows infected tissue treated with PC786 basally in the well media. Both images were taken 5dpi.

References

Anderson, E. J., Carosone-Link, P., Yogev, R., Yi, J., & Simoes, E. A. F. (2017). Effectiveness of Palivizumab in High-risk Infants and Children: A Propensity Score Weighted Regression Analysis. *Pediatr Infect Dis J, 36*(8), 699-704. doi:10.1097/INF.0000000000001533

Bai, J., Smock, S. L., Jackson, G. R., Jr., MacIsaac, K. D., Huang, Y., Mankus, C., . . . Hayden, P. J. (2015). Phenotypic responses of differentiated asthmatic human airway epithelial cultures to rhinovirus. *PLoS One, 10*(2), e0118286. doi:10.1371/journal.pone.0118286

Bissell, M. J., Hall, H. G., & Parry, G. (1982). How does the extracellular matrix direct gene expression? *J Theor Biol., 99*, 31-68.

Blount, R. E., Jr., Morris, J. A., & Savage, R. E. (1956). Recovery of cytopathogenic agent from chimpanzees with coryza. *Proc Soc Exp Biol Med, 92*(3), 544-549.

Brand, H. K., Ferwerda, G., Preijers, F., de Groot, R., Neeleman, C., Staal, F. J., . . . Hermans, P. W. (2013). CD4+ T-cell counts and interleukin-8 and CCL-5 plasma concentrations discriminate disease severity in children with RSV infection. *Pediatr Res, 73*(2), 187-193. doi:10.1038/pr.2012.163

Brookes, D., Coates, M., Allen, H., Ayrton, J., Davis, A., Hows, M., . . . Ito, K. (2016). LATE-BREAKING ABSTRACT: Effects of a single treatment with PC786, a novel inhibitor of respiratory syncytial virus replication, on viral load and biomarkers in fully differentiated human bronchial epithelial cells. Paper presented at the 10.1 Respiratory Infections.

Brookes, D. W., Coates, M., Allen, H., Daly, L., Constant, S., Huang, S., . . . Ito, K. (2018). Late therapeutic intervention with a respiratory syncytial virus L-protein

polymerase inhibitor, PC786, on respiratory syncytial virus infection in human airway epithelium. Br J Pharmacol, 175(12), 2520-2534. doi:10.1111/bph.14221

Bueno, S. M., Gonzalez, P. A., Riedel, C. A., Carreno, L. J., Vasquez, A. E., & Kalergis, A. M. (2011). Local cytokine response upon respiratory syncytial virus infection. *Immunol Lett, 136*(2), 122-129. doi:10.1016/j.imlet.2010.12.003

Centers for Disease Control and Prevention. (2018a). RSV in Infants and Young Children. Retrieved from https://www.cdc.gov/rsv/high-risk/infants-young-children.html

Centers for Disease Control and Prevention. (2018b). RSV in Older Adults and Adults with Chronic Medical Conditions. Retrieved from https://www.cdc.gov/rsv/high-risk/older- adults.html

Chapman, J., Abbott, E., Alber, D. G., Baxter, R. C., Bithell, S. K., Henderson, E. A., . . . Powell, K. L. (2007). RSV604, a novel inhibitor of respiratory syncytial virus replication. Antimicrob Agents Chemother, 51(9), 3346-3353. doi:10.1128/AAC.00211-07

Chen, Y. W., Huang, S. X., de Carvalho, A., Ho, S. H., Islam, M. N., Volpi, S., . . . Snoeck, H. W. (2017). A three-dimensional model of human lung development and disease from pluripotent stem cells. *Nat Cell Biol, 19*(5), 542-549. doi:10.1038/ncb3510

Chen, Y. X., Xie, G. C., Pan, D., Du, Y. R., Pang, L. L., Song, J. D., . . . Hu, B. R. (2018). Three- dimensional Culture of Human Airway Epithelium in Matrigel for Evaluation of Human Rhinovirus C and Bocavirus Infections. Biomed Environ Sci, 31(2), 136-145. doi:10.3967/bes2018.016

Chun, Y. H., Park, J. Y., Lee, H., Kim, H. S., Won, S., Joe, H. J., . . . Lee, J. S. (2013). Rhinovirus-Infected Epithelial Cells Produce More IL-8 and RANTES Compared With Other Respiratory Viruses. Allergy Asthma Immunol Res, 5(4), 216-223. doi:10.4168/aair.2013.5.4.216

Coates, M., Brookes, D., Kim, Y. I., Allen, H., Fordyce, E. A. F., Meals, E. A., . . . Rapeport, G. (2017). Preclinical Characterization of PC786, an Inhaled Small-Molecule Respiratory Syncytial Virus L Protein Polymerase Inhibitor. Antimicrob Agents Chemother, 61(9). doi:10.1128/AAC.00737-17

Coppeta, J. R., Mescher, M. J., Isenberg, B. C., Spencer, A. J., Kim, E. S., Lever, A. R., . . . Borenstein, J. T. (2016). A portable and reconfigurable multi-organ platform for drug development with onboard microfluidic flow control. Lab Chip, 17(1), 134-144. doi:10.1039/c6lc01236a

Deval, J., Hong, J., Wang, G., Taylor, J., Smith, L. K., Fung, A., . . . Beigelman, L. (2015). Molecular Basis for the Selective Inhibition of Respiratory Syncytial Virus RNA Polymerase by 2'-Fluoro-4'-Chloromethyl-Cytidine Triphosphate. PLoS Pathog, 11(6), e1004995. doi:10.1371/journal.ppat.1004995

Donalisio, M., Rusnati, M., Cagno, V., Civra, A., Bugatti, A., Giuliani, A., . . . Lembo, D. (2012). Inhibition of human respiratory syncytial virus infectivity by a dendrimeric heparan sulfate-binding peptide. *Antimicrob Agents Chemother, 56*(10), 5278-5288. doi:10.1128/AAC.00771-12

Edmondson, R., Broglie, J. J., Adcock, A. F., & Yang, L. (2014). Three-dimensional cell culture systems and their applications in drug discovery and cell-based biosensors. *Assay Drug Dev Technol, 12*(4), 207-218. doi:10.1089/adt.2014.573

Garcia-Garcia, M. L., Calvo, C., Moreira, A., Canas, J. A., Pozo, F., Sastre, B., . . . Del Pozo, V. (2017). Thymic stromal lymphopoietin, IL-33, and periostin in hospitalized infants with viral bronchiolitis. *Medicine (Baltimore), 96*(18), e6787. doi:10.1097/MD.0000000000006787

Goodwin, T. J., McCarthy, M., Cohrs, R. J., & Kaufer, B. B. (2015). 3D tissue-like assemblies: A novel approach to investigate virus-cell interactions. *Methods, 90*, 76-84. doi:10.1016/j.ymeth.2015.05.010

Guerrero-Plata, A., Baron, S., Poast, J. S., Adegboyega, P. A., Casola, A., & Garofalo, R. P. (2005). Activity and regulation of alpha interferon in respiratory syncytial virus and human metapneumovirus experimental infections. J Virol, 79(16), 10190-10199. doi:10.1128/JVI.79.16.10190-10199.2005

Han, J., Dakhama, A., Jia, Y., Wang, M., Zeng, W., Takeda, K., . . . Gelfand, E. W. (2012). Responsiveness to respiratory syncytial virus in neonates is mediated through thymic stromal lymphopoietin and OX40 ligand. *J Allergy Clin Immunol, 130*(5), 1175-1186 e1179. doi:10.1016/j.jaci.2012.08.033

Harcourt, J., Alvarez, R., Jones, L. P., Henderson, C., Anderson, L. J., & Tripp, R. A. (2006). Respiratory syncytial virus G protein and G protein CX3C motif adversely affect CX3CR1+ T cell responses. *J Immunol, 176*(3), 1600-1608. doi:10.4049/jimmunol.176.3.1600

Henderson EA, Alber DG, Baxter RC, Bithell SK, Budworth J, Carter MC, Chubb A, Cockerill GS, Dowdell VC, Fraser IJ, Harris RA, Keegan SJ, Kelsey RD, Lumley JA, Stables JN, Weerasekera N, Wilson LJ, Powell KL (2007) 1,4-benzodiazepines as inhibitors of respiratory syncytial virus. The identification of a clinical candidate. J Med Chem 50 (7):1685-1692. doi:10.1021/jm060747l

Huang, S., Boda, B., Bonfante, R., Vernaz, J., Alouani, P., & Constant, S. (2018). Late Breaking Abstract - Efficient replication of respiratory syncytial virus induces a decrease of mucociliary clearance in human small airway 3D culture. *European Respiratory Journal, 52*(Supplement 62), PA5449. doi:10.1183/13993003.congress-2018.PA5449

Huh, D., Matthews, B. D., Mammoto, A., Montoya-Zavala, M., Hsin, H. Y., & Ingber, D. E. (2010). Reconstituting organ-level lung functions on a chip. *Science, 328*(5986), 1662- 1668. doi:10.1126/science.1188302

Jung, K. H., Choi, J. A., Westover, J., Smee, D., & Day, C. (2016). *Antiviral Activity of Ribavirin, 2',3'-Dideoxicitidine, Pirodavir, Oseltamivir and Infergen Against RSV, Adeno-2, Rhino-14, Influenza and MERS Virus Infection in Differentiated Normal Bronchial Epithelial (NHBE) Cells.* Paper presented at the 29th International Conference on Antiviral Research, La Jolla California.

Kim K. Tekkanat, H. M., Allison Miller, Aaron A. Berlin, Steven L. Kunkel, Nicholas W. Lukacs. (2002). RANTES (CCL5) production during primary respiratory syncytial virus infection exacerbates airway disease. *European Journal of Immunology, 32*, 3276-3284.

Krilov, L. R. (2002). Safety issues related to the administration of ribavirin. *Pediatr Infect Dis J, 21*(5), 479-481.

Laham, F. R., Mansbach, J. M., Piedra, P. A., Hasegawa, K., Sullivan, A. F., Espinola, J. A., & Camargo, C. A., Jr. (2017). Clinical Profiles of Respiratory Syncytial Virus Subtypes A AND B Among Children Hospitalized with Bronchiolitis. *Pediatr Infect Dis J, 36*(8), 808-810. doi:10.1097/INF.0000000000001596

Lopez-Guisa, J. M., Powers, C., File, D., Cochrane, E., Jimenez, N., & Debley, J. S. (2012). Airway epithelial cells from asthmatic children differentially express proremodeling factors. *J Allergy Clin Immunol, 129*(4), 990-997 e996. doi:10.1016/j.jaci.2011.11.035

Mackman, R. L., Sangi, M., Sperandio, D., Parrish, J. P., Eisenberg, E., Perron, M., . . . Cihlar, T. (2015). Discovery of an oral respiratory syncytial virus (RSV) fusion inhibitor (GS-5806) and clinical proof of concept in a human RSV challenge study. J Med Chem, 58(4), 1630-1643. doi:10.1021/jm5017768

MatTek Corporation. (2014). EpiAirway, EpiVaginal, EpiOral, EpiOcular, and EpiIntestinal tissues. In. Isolation of Total RNA from MatTek Tissue Models Protocol: MatTek Corporation.

MatTek Corporation. (2019a). Respiratory Infection. Retrieved from https://www.mattek.com/application/respiratory-infection/

MatTek Corporation. (2019b). Tissue Model EpiAirway. Retrieved from https://www.mattek.com/products/epiairway/

MatTek Corporation. (2019c). Figure 2. In. Protocol: Extended Culture Times - Use for Culture Stand/Washers/Hanging Tops: MatTek Corporation.

McAllister, C. S., Ansaldi, D., Growcott, E. J., Zhong, Y., Quackenbush, D., Wolff, K. C., . . . Kuhen, K. L. (2020). Dexamethasone inhibits respiratory syncytial virus-driven mucus production while increasing viral replication without altering antiviral interferon signaling. Virology, 540, 195-206. doi:10.1016/j.virol.2019.10.007

Mirabelli, C., Jaspers, M., Boon, M., Jorissen, M., Koukni, M., Bardiot, D., . . . Jochmans, D. (2018). Differential antiviral activities of respiratory syncytial virus (RSV) inhibitors in human airway epithelium. *J Antimicrob Chemother, 73*(7), 1823-1829. doi:10.1093/jac/dky089

Mishra, D. K., Sakamoto, J. H., Thrall, M. J., Baird, B. N., Blackmon, S. H., Ferrari, M., . . . Kim, M. P. (2012). Human lung cancer cells grown in an ex vivo 3D lung model produce matrix metalloproteinases not produced in 2D culture. *PLoS One, 7*(9), e45308. doi:10.1371/journal.pone.0045308

Palermo, L. M., Uppal, M., Skrabanek, L., Zumbo, P., Germer, S., Toussaint, N. C., . . . Moscona, A. (2016). Features of Circulating Parainfluenza Virus Required for Growth in Human Airway. *MBio, 7*(2), e00235. doi:10.1128/mBio.00235-16

Palmer, S. G., DeVito, I., Jenkins, S. G., Niewiesk, S., Porotto, M., & Moscona, A. (2014). Circulating clinical strains of human parainfluenza virus reveal viral entry requirements for in vivo infection. *J Virol, 88*(22), 13495-13502. doi:10.1128/JVI.01965-14

Perron, M., Stray, K., Kinkade, A., Theodore, D., Lee, G., Eisenberg, E., . . . Cihlar, T. (2015). GS-5806 Inhibits a Broad Range of Respiratory Syncytial Virus Clinical Isolates by Blocking the Virus-Cell Fusion Process. Antimicrob Agents Chemother, 60(3), 1264-1273. doi:10.1128/AAC.01497-15

Rhodin, M., McAllister, N., Castillo, J., Kim, I. J., Yu, J., Or, Y. S., . . . Lin, K. (2018). *EDP- 938, a Novel Non-Fusion Replication Inhibitor of RSV, Displays a High Barrier to Resistance In Vitro.* Presented at the 11th International Respiratory Syncytial Virus Symposium, Asheville, North Carolina.

Rhodin, M., McAllister, N., Kim, I. J., Yu, J., Blaisdell, T., Panarese, J., . . . Or, Y. S. (2016). *EP-023938, A Novel Non-Fusion Replication Inhibitor of Respiratory Syncytial Virus (RSV).* Presented at the 10th Annual Respiratory Syncytial Virus conference, Patagonia, Argentina.

Roe, M. F., Bloxham, D. M., Cowburn, A. S., & O'Donnell, D. R. (2011). Changes in helper lymphocyte chemokine receptor expression and elevation of IP-10 during acute respiratory syncytial virus infection in infants. *Pediatr Allergy Immunol, 22*(2), 229-234. doi:10.1111/j.1399-3038.2010.01032.

Rojas-Ramos, E., Avalos, A. F., Perez-Fernandez, L., Cuevas-Schacht, F., Valencia-Maqueda, E., & Teran, L. M. (2003). Role of the chemokines RANTES, monocyte chemotactic proteins-3 and -4, and eotaxins-1 and -2 in childhood asthma. *Eur Respir J, 22*(2), 310-316. doi:10.1183/09031936.03.00084802

Rose, E. B., Wheatley, A., Langley, G., Gerber, S., & Haynes, A. (2018). Respiratory Syncytial Virus Seasonality - United States, 2014-2017. *MMWR Morb Mortal Wkly Rep, 67*(2), 71- 76. doi:10.15585/mmwr.mm6702a4

Sachs, N., Papaspyropoulos, A., Zomer-van Ommen, D. D., Heo, I., Bottinger, L., Klay, D., . . . Clevers, H. (2019). Long-term expanding human airway organoids for disease modeling. *EMBO J, 38*(4). doi:10.15252/embj.2018100300

Sananez, I., Raiden, S., Erra-Diaz, F., De Lillo, L., Holgado, M. P., Geffner, J., & Arruvito, L. (2018). Dampening of IL-2 Function in Infants With Severe Respiratory Syncytial Virus Disease. *J Infect Dis, 218*(1), 75-83. doi:10.1093/infdis/jiy180

Sanyal, S. (2010). Culture and Assay Systems Used for 3D Cell Culture. Retrieved from
https://www.corning.com/catalog/cls/documents/application-
notes/an_245_culture_and_assay_systems_used_for_3D_cell_culture.pdf

Saravia, J., You, D., Shrestha, B., Jaligama, S., Siefker, D., Lee, G. I., . . . Cormier, S. A.
(2015). Respiratory Syncytial Virus Disease Is Mediated by Age-Variable IL-33.
PLoS Pathog, 11(10), e1005217. doi:10.1371/journal.ppat.1005217

Science, M., Akseer, N., Asner, S., & Allen, U. (2019). Risk stratification of
immunocompromised children, including pediatric transplant recipients at risk of
severe respiratory syncytial virus disease. *Pediatric Transplantation*.
doi:10.1111/petr.13336

Shi, T., McAllister, D. A., O'Brien, K. L., Simoes, E. A. F., Madhi, S. A., Gessner, B. D.,
. . . Nair, H. (2017). Global, regional, and national disease burden estimates of
acute lower respiratory infections due to respiratory syncytial virus in young
children in 2015: a systematic review and modelling study. *The Lancet,
390*(10098), 946-958. doi:10.1016/s0140-6736(17)30938-8

Sigurs, N., Bjarnason, R., Sigurbergsson, F., & Kjellman, B. (2000). Respiratory
syncytial virus bronchiolitis in infancy is an important risk factor for asthma and
allergy at age 7. *Am J Respir Crit Care Med, 161*(5), 1501-1507.
doi:10.1164/ajrccm.161.5.9906076

Stier, M. T., Bloodworth, M. H., Toki, S., Newcomb, D. C., Goleniewska, K., Boyd, K.
L., . . . Peebles, R. S., Jr. (2016). Respiratory syncytial virus infection activates
IL-13-producing group 2 innate lymphoid cells through thymic stromal
lymphopoietin. J Allergy Clin Immunol, 138(3), 814-824 e811.
doi:10.1016/j.jaci.2016.01.050

Tabarani, C. M., Bonville, C. A., Suryadevara, M., Branigan, P., Wang, D., Huang, D., . .
. Domachowske, J. B. (2013). Novel inflammatory markers, clinical risk factors
and virus type associated with severe respiratory syncytial virus infection. *Pediatr
Infect Dis J, 32*(12), e437-442. doi:10.1097/INF.0b013e3182a14407

Taylor, G. (2017). Animal models of respiratory syncytial virus infection. *Vaccine, 35*(3), 469- 480. doi:10.1016/j.vaccine.2016.11.054

The IMpact-RSV Study Group. (1998). Palivizumab, a humanized respiratory syncytial virus monoclonal antibody, reduces hospitalization from respiratory syncytial virus infection in high-risk infants. *Pediatrics, 102*(3 Pt 1), 531-537.

Vazquez, Y., Gonzalez, L., Noguera, L., Gonzalez, P. A., Riedel, C. A., Bertrand, P., & Bueno, S. M. (2019). Cytokines in the Respiratory Airway as Biomarkers of Severity and Prognosis for Respiratory Syncytial Virus Infection: An Update. *Front Immunol, 10*, 1154. doi:10.3389/fimmu.2019.01154

Weiss, K. A., Christiaansen, A. F., Fulton, R. B., Meyerholz, D. K., & Varga, S. M. (2011). Multiple CD4+ T cell subsets produce immunomodulatory IL-10 during respiratory syncytial virus infection. *J Immunol, 187*(6), 3145-3154. doi:10.4049/jimmunol.1100764

Wu, X., Peters-Hall, J. R., Bose, S., Pena, M. T., & Rose, M. C. (2011). Human bronchial epithelial cells differentiate to 3D glandular acini on basement membrane matrix. *Am J Respir Cell Mol Biol, 44*(6), 914-921. doi:10.1165/rcmb.2009-0329OC

Xu, R., Palmer, S. G., Porotto, M., Palermo, L. M., Niewiesk, S., Wilson, I. A., & Moscona, A. (2013). Interaction between the hemagglutinin-neuraminidase and fusion glycoproteins of human parainfluenza virus type III regulates viral growth in vivo. *MBio, 4*(5), e00803- 00813. doi:10.1128/mBio.00803-13

Ying, S., O'Connor, B., Ratoff, J., Meng, Q., Mallett, K., Cousins, D., . . . Corrigan, C. (2005). Thymic stromal lymphopoietin expression is increased in asthmatic airways and correlates with expression of Th2-attracting chemokines and disease severity. *J Immunol, 174*(12), 8183-8190. doi:10.4049/jimmunol.174.12.8183